AD NUMBER

AD805410

NEW LIMITATION CHANGE

TO

Approved for public release, distribution unlimited

FROM

Distribution authorized to U.S. Gov't. agencies and their contractors; Administrative/Operational use; 31 Dec 1966. Other requests shall be referred to Air Force Rocket Propulsion Lab, Edwards AFB CA.

AUTHORITY

AFRPL, Ltr, 20 Dec 1971

DOWNEY PLANT

ORDNANCE DIVISION

PROJECT SOPHY

SOLID PROPELLANT HAZARDS PROGRAM

Technical Documentary Report No.
AFRPL-TR-66-276

Progress Report On
Contract AF 04(611)-10919

Report Number 0977-01(05)QP / December 1966 / Copy 76

AEROJET GENERAL TIRE GENERAL

AEROJET-GENERAL CORPORATION
Ordnance Division
11711 Woodruff Avenue
Downey, California

PROGRESS REPORT

PROJECT SOPHY

SOLID PROPELLANT HAZARDS PROGRAM

Technical Documentary Report No.
AFRPL-TR-66-~~26~~ 276

Contract AF 04(611)-10919

0977-01(05)QP

Period Covered: 1 September 1966 - 30 November 1966

R. B. Elwell
O. R. Irwin
Prepared by: R. W. Vail, Jr. Date: 31 December 1966

Reviewed by: M. Nishibayashi
M. Nishibayashi, Head
Explosive Kinetics Dept.

No. of Pages: 80

Approved by: A. Wheeler, for
H. J. Fisher, Manager
Research Division

Classification: UNCLASSIFIED

FOREWORD

This report was prepared by Aerojet-General Corporation, Downey California, on Air Force Contract AF 04(611)-10919, which supports the USAF Solid Propellant Hazards Study Program (Project SOPHY), Project 63A00201. The period covered by this report is 1 September 1966 through 30 November 1966.

ABSTRACT

A correlation is reported that evaluates the ise by the Aerojet detonation model of the modified Jones mode , to describe non-ideal detonation characteristics of solid-con posite propellant.

An analysis of the perturbation of the detona ion process in hollow cylindrical charges is presented. The critic al geometries of triangular and rectangular columns have bee found to be 95% and 94% of the critical diameter, respectively. The pseudocritical geometries (defined in this report) for circu ar-core and cross-core hollow cylinders both are 88% of the cr tical diameter. The Hugoniot of AAB-3225 propellant (adulterate propellant containing 7.1% RDX) is reported. A generalized expre ssion for the effective grain radius has been developed. Corrected values of the peak overpressure data from the two large critica l diameter tests of unadulterated propellant (72- and 60-in. d ameter) are reported. Progress has been made in determi ning the effects of several processing parameters on the quality of cast porous propellant. Techniques to measure the surf ce area of cracked propellant samples are being evaluated.

CONTENTS

ILLUSTRATIONS

TABLES

TABLES (Cont)

1. INTRODUCTION

This quarterly report is the fifth of a series of reports partially fulfilling Contract AF 04(611)-10919, Large Solid-Propellant Boosters Explosive Hazards Study Program. The purpose of this program is to gain additional knowledge and to develop new techniques for analyzing the explosive hazard and damage potential of large solid-propellant rocket motors.

The objectives of this program are: (1) to determine the influence of grain shape on propellant detonability and sensitivity, (2) to determine the critical diameter of a typical solid-composite rocket-motor propellant, (3) to determine what changes a solid-propellant grain might undergo when exposed to operational mishaps, and (4) to develop methods to simulate and characterize these changes.

2. SUMMARY

A correlation has been made to determine the validity of applying the modified Jones detonation model in developing the Aerojet model for critical diameter as a function of RDX content. The results indicate that complete correlation will require analyses of detonation velocity vs diameter data from more than one adulterated propellant formulation. These data are not yet available, but they will be acquired from the card-gap sensitivity tests that will be conducted under this program.

The abnormal detonation behavior of shock-initiated hollow cylindrical samples appears to be caused by deflagrative erosion of the inner surface of the samples, owing to the high-velocity jet that is formed in the perforation by Mach interaction of the shock waves produced by the detonating material.

The critical geometries of solid triangular columns and rectangular slabs are 95% and 94% of the critical diameter, respectively.

The pseudocritical geometries of circular-core and cross-core hollow cylinders both are 88% of the critical diameter.

The Hugoniot of AAB-3225 (7.1% RDX) adulterated propellant is $P = 62.75\,\mu^2 + 27.38\,\mu$. The correct Hugoniot for AAB-3189 is $P = 47.80\,\mu^2 + 32.18\,\mu$. This correction of the Hugoniot reported in SOPHY I is facilitated by an improvement in the method by which the data are reduced.

A generalized expression has been developed for the effective grain radius, which is used in the detonation model. The new expression will handle hot-spot initiation sites of any type, number, and size.

Peak overpressure data from the 72-in.-diameter critical-diameter test (CD-96) and the 60-in.-diameter critical-diameter test (CD-98) have been corrected. Their final values are reported.

Progress in the synthesis and analysis of porous and cracked propellant is discussed. Various processing parameters are evaluated regarding their influence on the quality of porous propellant.

3. THEORY OF CRITICAL GEOMETRY

3.1 TECHNICAL DISCUSSION - PHASE I SUBTASKS

3.1.1 Variance and Mean Critical Geometry (Subtask 3.2.1*)

The tests specifically designated for this subtask were completed earlier in the year. The analyses of their results were reported in the preceding quarterly report (Reference 2). The statistical estimate of the mean critical diameter was 2.66 in., for an adulterated AP-PBAN propellant that contains 9.2 % by weight RDX (Aerojet formulation AAB-3189). Data from SOPHY I, Contract AF 04(611)-9945, and SOPHY II Contract AF 04(611)-10919, were combined to yield this value of the mean critical diameter. The average standard deviation of the data was 0.08 in., which contained the within-batch standard deviation of 0.04 in. and the between-batch standard deviation of 0.07 in.

Since AAB-3189 is used in several subtasks of this program, additional critical-diameter data are available from the batch-control tests, which were performed with samples from each propellant batch. For example, in the critical geometry subtask (Phase 2, Subtask 3.3.2) the accuracy of the theory is estimated by comparing the critical geometry of each of several shapes with the critical diameter of the propellant

*Subtask number corresponds to the paragraph number in the program plan (Reference 1), which locates the description of that particular series of tests.

used. It is necessary, therefore, to obtain an estimate of the critical diameter from each batch. More precisely, it must be assured that the propellant does not significantly differ from prior batches of the same formulation. To establish this, in each batch there are included eight solid-cylindrical batch-control samples of which two in each batch have nominal diameters of 2.56, 2.63, 2.69, and 2.75 in.

Propellant Batch 4EH-108, which included triangular samples for the critical geometry subtask and hollow cylinders for the jetting phenomena study (Subtask 3.2.4), had a critical diameter of 2.73 in. This value is consistent with the estimates derived from the previous data. Combining the results of the Batch 4EH-108 tests with all previous data changes the estimated mean critical diameter of AAB-3189 to 2.69 in., but does not affect the estimate of the standard deviation of 0.08 in.

Batches 4EH-109 and -110 contained samples for the critical geometry subtask (rectangular cross-section and hollow cylinders). The results of the batch-control tests from batches were negative; i.e., no detonation occurred in samples of up to 2.75 in. nominal diameter. These batches differ significantly from all previously tested batches of AAB-3189. The critical diameters of these two batches were found by testing larger diameter samples, which were prepared by turning down several samples that were originally destined for use in Subtask 3.3.1.* The critical diameter of Batch 4EH-109 was found to be between 2.95 and 3.00 in. The critical diameter of Batch 4EH-110 was between 2.90 and 2.95 in.

Careful study of the batch mixing records does not show cause for the anomalous behavior of these batches. Since the samples cast were destined for use in the critical geometry subtask, they were allowed to qualify for testing because the test results could be compared to the individual critical diameters of these batches and they did not need to be compared directly with data obtained from other AAB-3189 tests.

The results of the batch-control tests for Batches 4EH-108, -109, and -110 are shown in Table 1.

*These samples had already been cast when the decision was made to not perform this subtask, because of the positive results of Subtask 3.2.3 (Section 3.1.3). Therefore their alteration does not affect the SOPHY II program.

Table 1. Batch-Control Tests, AAB-3189 Propellant.

Batch No.	Diameter (in.)	Result	Test No.
4EH-108	2.55	No-Go	3.2.1.175
4EH-108	2.54	No-Go	3.2.1.176
4EH-108	2.62	No-Go	3.2.1.177
4EH-108	2.62	No-Go	3.2.1.178
4EH-108	2.67	No-Go	3.2.1.179
4EH-108	2.67	No-Go	3.2.1.180
4EH-108	2.73	Go	3.2.1.181
4EH-108	2.74	No-Go	3.2.1.182
4EH-109	2.73	No-Go	3.2.1.183
4EH-109	2.73	No-Go	3.2.1.184
4EH-109	2.80	No-Go	3.2.1.187
4EH-109	2.90	No-Go	3.2.1.188
4EH-109	2.95	No-Go	3.2.1.191
4EH-109	3.00	Go	3.2.1.192
4EH-110	2.73	No-Go	3.2.1.185
4EH-110	2.73	No-Go	3.2.1.186
4EH-110	2.90	No-Go	3.2.1.189
4EH-110	2.95	Go	3.2.1.190

3.1.2 Mean Critical Diameter and Variance (Subtask 3.2.2)

Critical diameter determinations for AAB-3225, which is an AP-PBAN propellant adulterated with 7.1 % by weight RDX, exhibited a variation similar to that found with AAB-3189 (Section 3.1.1). The critical diameters of Batches 4EH-44 was 5.21 in., 4EH-107 was 5.25 in., and 4EH-84 was 6.36 in. The average densities of these batches were 1.735, 1.724, and 1.729 gm/cc, respectively. No indication of mixing or casting differences between batches was discovered. Since the density data do not correlate with the critical-diameter data, the difficulty has not been resolved. However, because of the agreement between Batches 4EH-44 and -107, it was concluded that Batch 4EH-84 was not representative of the AAB-3225 formulation.

The use of this type of propellant in the verification tests (Subtask 3.3.3) and in the sensitivity tests (Subtask 3.3.5) will provide further data by which the true critical diameter may be chosen. The verification tests include batch-control samples. The sensitivity tests include samples of 6-in. diameters and larger.

3.1.3 Detonation Velocity as a Function of Size (Subtask 3.2.3)

The Jones theory (Reference 3), originally developed to describe the nonideal detonation behavior of explosives, was needed in the development of the SOPHY detonation model to describe the variation in critical diameter of an RDX-adulterated composite propellant with changes in RDX content (Reference 4). The experimental data used to guide the development of the model were obtained in tests with samples having diameters nearly the same as the critical diameters. Data are needed regarding the variation of detonation velocity for different shapes over a large range of sizes to test the ability of the Jones theory and the model to describe the nonideal detonation behavior of composite propellants. These data also will be used to determine the relationship between detonation velocity, reaction-zone thickness, and size as a function of sample shape.

Detonation-velocity and conductance-zone measurements for AAB-3189 propellant were reported in Reference 2. It was stated that the thickness of the highly ionized region following the shock wave in composite propellant may be greater than the reaction zone itself. Since the probe instrumentation was providing data on the thickness of this conductance zone, no actual measure of the reaction-zone thickness was achieved if this interpretation is correct.

An alternative method to evaluate the use of the modified Jones theory involves only the detonation velocity-vs-size data. A series of calculations have been made to judge the correlation between measured and predicted diameters as functions of detonation velocity. The analysis is applied to two shapes: the circular cylinders and the square columns.

The Aerojet detonation model (Reference 4) is expressed by

$$d = \frac{\frac{3}{4} K_J^{1/2} \left(\frac{d_{RDX}}{2}\right)\left[\left(\frac{G}{f+c}\right)^{1/3} - 1\right] D}{B\left[1 - (D/D_i)^2\right]^{1/2}} \qquad (1)$$

where

d = charge diameter

K_J = the constant in the Jones expression, left unspecified in the Aerojet model

d_{RDX} = average RDX particle diameter

G = a constant, unspecified

f = wt fraction RDX

c = equivalent wt fraction RDX for other initiation sites

D = detonation velocity

B = linear burning rate of ammonium perchlorate (AP)

D_i = ideal detonation velocity

The AP burning rate can be expressed as a function of T_s, the surface temperature of the regressing AP, by

$$B = 2.1 \times 10^{-4} T_s \exp(-21,500/T_s) \qquad (2)$$

and T_s by

$$T_s = 1824 + 18.4 \rho_o D^2 - 0.137 \rho_o^2 D^4 \qquad (3)$$

where ρ_o is the AP bulk density. Thus d can be related uniquely to D if d_{RDX} and f are fixed. In this case, Equation 1 can be written

$$d = K\, g(f) \tag{4}$$

where

$$K = 3/4\, K_J^{1/2} \left(\frac{d_{RDX}}{2}\right) \left[\left(\frac{G}{f+c}\right)^{1/3} - 1\right] \tag{5}$$

and

$$g(f) = \frac{D}{B\left[1 - (D/D_i)^2\right]^{1/2}} \tag{6}$$

Therefore with D, d data, and an estimate of D_i it is possible to compute g(f) from Equations 2, 3, and 6. If the detonation model is applicable to nonideal detonation, a plot of d vs g(f) should produce a straight line with slope K.

The indicated correlation was carried out for AAB-3189 propellant, using data obtained under this subtask (reported in Reference 2) for both circular cylinders and square columns. A computer program carried out the computations of Equations 2, 3, and 6 and determined K by two methods: (1) by calculating the best value (denoted K_c) from the critical dimension and the critical detonation velocity estimates, and (2) by computing the least-squares best fit, denoted $\bar{K}$, from all the data. Equation 4 could possibly be fit best with an additive constant, so a third value of K (denoted K*) was calculated for a fit to

$$d = K^* g(f) + C^* \tag{7}$$

where C* is the finite intercept.

The results of these calculations are shown in Table 2. The "residual variance" estimates give a measure of how well the "best" values of K actually fit the data. Table 2 reveals that the fit of Equation 7 is considerably superior to that of Equation 4. Although there are no residual variance estimates for Equation 4 using the critical values, a plot of g(f) vs d (and s, the side of the square columns) using K_c yields a poor fit to the data. It may be assumed, therefore, that the best correlation of the nonideal detonation data for AAB-3189 is represented by Equation 7.

Table 2. Correlation of Aerojet Detonation Model in the Nonideal Region for AAB-3189 Propellant.

SQUARE COLUMNS

Equation	Slope (in.)	Intercept (in.)	Residual Variance ($in.^2$)
$s = \bar{K}\, g\,(f)$	$\bar{K} = 3.03 \times 10^{-4}$	---	5.31
$s_c = \bar{K}\, g_c(f)$	$K_c = 8.08 \times 10^{-4}$	---	---
$s = K^* g(f) + C^*$	$K^* = 18.8 \times 10^{-4}$	$C^* = -$	3.52 0.0092

CIRCULAR CYLINDERS

Equation	Slope (in.)	Intercept (in.)	Residual Variance ($in.^2$)
$d = \bar{K}\, g(f)$	$\bar{K} = 11.2 \times 10^{-4}$	---	2.01
$d_c = K_c\, g_c(f)$	$K_c = 8.73 \times 10^{-4}$	---	---
$d = K^* g(f) + C^*$	$K^* = 23.3 \times 10^{-4}$	$C^* = -$	1.87 0.197

Since this correlation differs from the assumed form (Equation 4), it is desirable to determine its effect when the Aerojet model is used to fit the critical diameter vs wt fraction RDX data generated on Contract AF 04(611)-9945 (Reference 4). At critical conditions, Equation 7 becomes

$$d_c = K^* g_c(f) + C^* \tag{8}$$

However, since it was shown that d_c is linearly dependent on $(1/f + c)^{1/3}$ (Reference 4) K* or C* may depend on $(1/f+c)^{1/3}$. Therefore, in the general case,

$$K^* = K^*_1 \left(\frac{1}{f+c}\right)^{1/3} + K^*_2 \tag{9}$$

$$C^* = C^*_1 \left(\frac{1}{f+c}\right)^{1/3} + C^*_2 \tag{10}$$

where K^*_1, K^*_2, C^*_1, and C^*_2 are constants independent of $(1/f+c)^{1/3}$.

Substituting Equations 9 and 10 into Equation 8 gives, after rearranging,

$$d_c = \left[K^*_1 g_c(f) + C^*_1\right]\left(\frac{1}{f+c}\right)^{1/3} + \left[K^*_2 g_c(f) + C^*_2\right] \tag{11}$$

Combining Equations 1 and 6, at the critical case, gives

$$d_c = \left[\frac{3}{4} K_J^{1/2} \left(\frac{d_{RDX}}{2}\right) G^{1/3} g_c(f)\right]\left(\frac{1}{f+c}\right)^{1/3} - \left[\frac{3}{4} K_J^{1/2} \left(\frac{d_{RDX}}{2}\right) g_c(f)\right] \tag{12}$$

For Equations 11 and 12 to be compatible the following must be true

$$K^*_1 g_c(f) + C^*_1 = \frac{3}{4} K_J^{1/2} \left(\frac{d_{RDX}}{2}\right) G^{1/3} g_c(f) \qquad (13)$$

$$K^*_2 g_c(f) + C^*_2 = \frac{3}{4} K_J^{1/2} \left(\frac{d_{RDX}}{2}\right) g_c(f) \qquad (14)$$

Since K_J, d_{RDX}, and G are constants, Equations 9, 10, 13, and 14 state that K^*_1, K^*_2, C^*_1, and C^*_2 depend only on $g_c(f)$. However, since it was found that $g_c(f)$ is itself a constant independent of f (Reference 4), the equations require that K^*_1, K^*_2, C^*_1, and C^*_2 be constants also independent of f. To determine if Equations 13 and 14 are satisfied, it is necessary to specify all these constants. However examination of Equations 9 and 10 shows that this cannot be done until other values of K* and C* are determined at other f's.

It may be concluded that the correlation found with Equation 7 is not inconsistent with the Aerojet detonation model if the compatibility conditions are met. When additional D vs d data become available from the tests in Subtask 3.3.5 a correlation can be attempted and new values of K* and C* can be determined. With this information and the data in Table 2, Equations 9 and 10 can be used to solve explicitly for K^*_1, K^*_2, C^*_1, and C^*_2. These values can then be substituted into Equations 13 and 14 to test compatibility. The values of the right-hand sides of Equation 13 and 14 and of $g_c(f)$ are known from the prior d_c-vs-f studies. It should be noted that Equations 13 and 14 must be satisfied for values of the constants determined from any pair of K*, C* data and must therefore hold for all RDX contents from $0 \leq f \leq 0.10$ if the Aerojet model is to be generally valid for nonideal detonation.

As noted above, the data in Table 2 show that the best correlation for solid squares is represented by Equation 7. Since d_c and s_c differ, a comparison of the results for cylinders and squares can be made by dividing Equation 7 (with the appropriate constants) by d_c and s_c respectively. This leads to

$$\frac{d}{d_c} = 8.63 \times 10^{-4}\, g(f) - 1.81 \qquad (15)$$

for cylinders, and

$$\frac{s}{s_c} = 7.55 \times 10^{-4}\, g(f) - 1.41 \qquad (16)$$

for solid squares.

Although these equations are now on an equivalent basis, and the respective constants are closer to each other than those in Table 2, it still is believed that significant differences between them do exist. Thus, it appears that even if Equation 1 is valid, for the same reasons discussed with respect to cylinders, the Jones theory cannot be applied directly to solid squares unless a value of K_J different from that determined for cylinders, is used in Equation 1. However, as D vs s data for propellant other than AAB-3189 become available, a more definitive determination of the applicability of the Jones theory to solid squares will be possible.

3.1.4 Jetting Phenomena Study (Subtask 3.2.4)

Streak-camera observations of previous critical geometry tests of hollow cylindrical samples showed that an abrupt cessation of an apparently steady detonation occurs at some point along the length of the sample (Reference 4). The location of this point appeared to be determined by the web thickness of the grain, when the results obtained for only one propellant formulation were analyzed. Since it is observed that a high-velocity jet is produced in the core of an end-initiated hollow cylinder, the responsibility for the anomalous behavior of hollow cylindrical samples may be ascribed to effects caused by the jetting phenomenon. Therefore, this subtask consists of a series of tests designed to investigate the manner in which jetting affects the detonation reaction of hollow cylinders. These tests include studies of the effect of core diameter (ID), and sample length, and web thickness on the behavior of hollow cylinders.

3.1.4.1 Effect of Core Diameter

Hollow samples, cast from AAB-3189 propellant, having web thickness equal to 1.4 in. were prepared in several sizes in which only the ID varied. Core diameters of 0.06, 0.12, 0.25, 0.50, 0.80, 1.5, and 3.0 in. were chosen. All sample lengths were four times the OD. The samples were instrumented with four sets of ionization probes in circuit

with four rasteroscillographs to obtain distance-time data on the reactive shock wave and the jet. Three sets of probes placed in the propellant gather the data at radial positions 1/4-, 1/2-, and 3/4-web in from the outside of the samples. The fourth set of probes monitors the travel of the jet along the charge axis. Figure 1 shows the test setup.

A 1-in.-thick Plexiglas plate is placed between the Composition B booster and the propellant acceptor. The Plexiglas attenuates the velocity of the shock wave entering the acceptor. This allows better resolution of the initial behavior of the reactive shock wave in the propellant by preventing its being masked by the normal attenuation of a highly overboostered initiating wave in the acceptor, which would occur if the booster charge were placed directly on the propellant sample. The Plexiglas barrier also prevents the booster shock wave from forming a jet in the hollow acceptor before the propellant detonation reaction produces its jet. The 1-in. thick attenuator does not reduce the shock pressure below the minimum level required to initiate detonation in these samples.

The specific purpose of these tests was to determine the influence of the ID on the location of the point along the charge length where detonation ceases. It is of interest to learn whether a minimum core diameter exists below which the jet has no effect on the propellant behavior, and whether a maximum core diameter of reasonable proportions exists above which the jet has no effect on the propellant behavior. The 3-in.-ID (the maximum core size tested) is not the largest that will be tested in this program. In the verification tests (Subtask 3.3.3) samples with 6-in. ID are included, which will permit further evaluation of the effect of core size.

The distance-vs-time data were reduced for plotting the detonation velocity vs distance along the sample at each radial distance into the sample.

Figure 2 is a plot of the data obtained at the 1/4-web depth. Only straight lines were used to connect the individual data points, because to have fit the data to smooth curves would have made it more difficult to isolate the data of any one sample size from the others. From these data it is evident that regardless of the size of the ID, the detonation began to fade after 7 in. of travel in the samples.

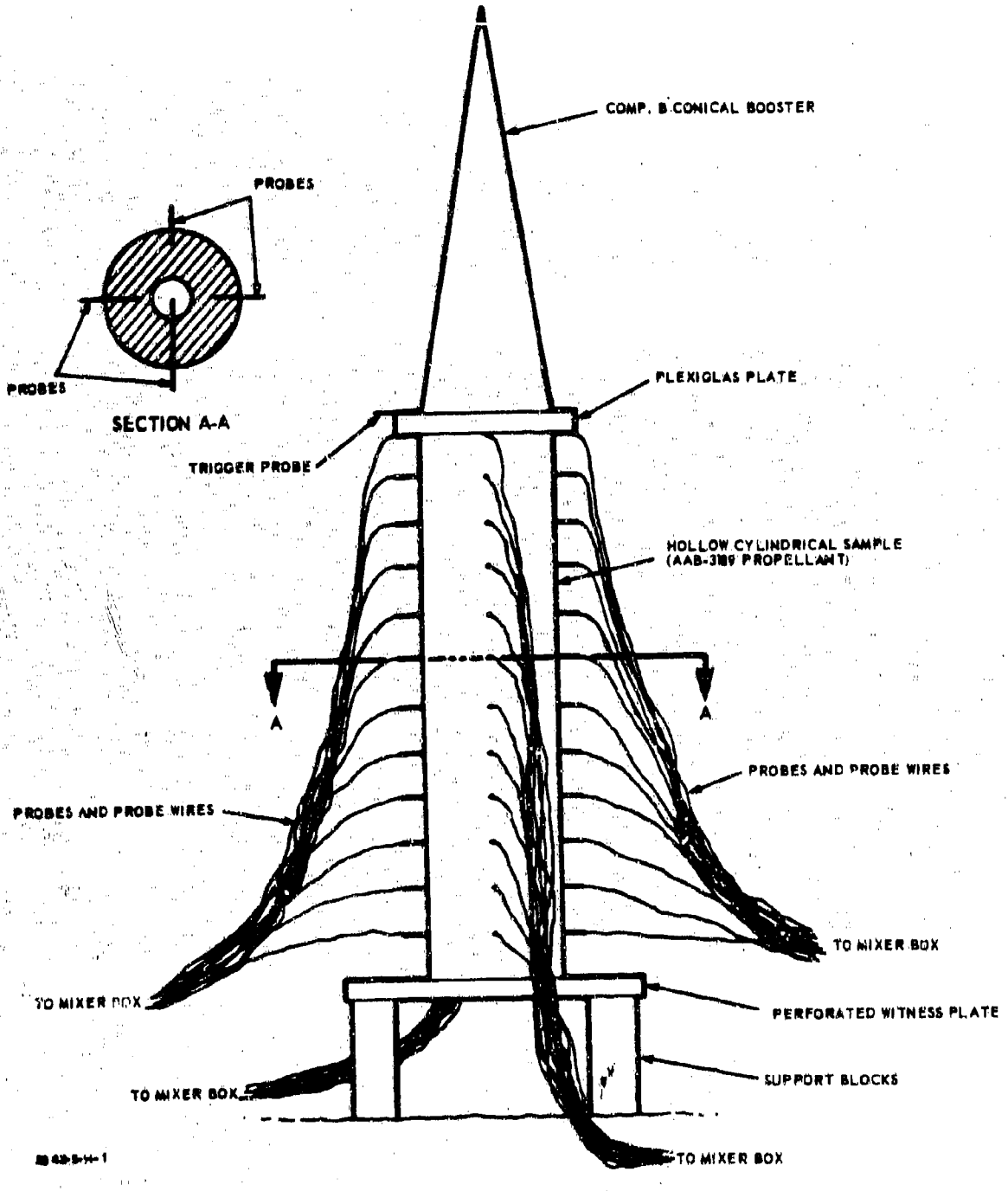

Figure 1. Jetting Phenomena Test Setup.

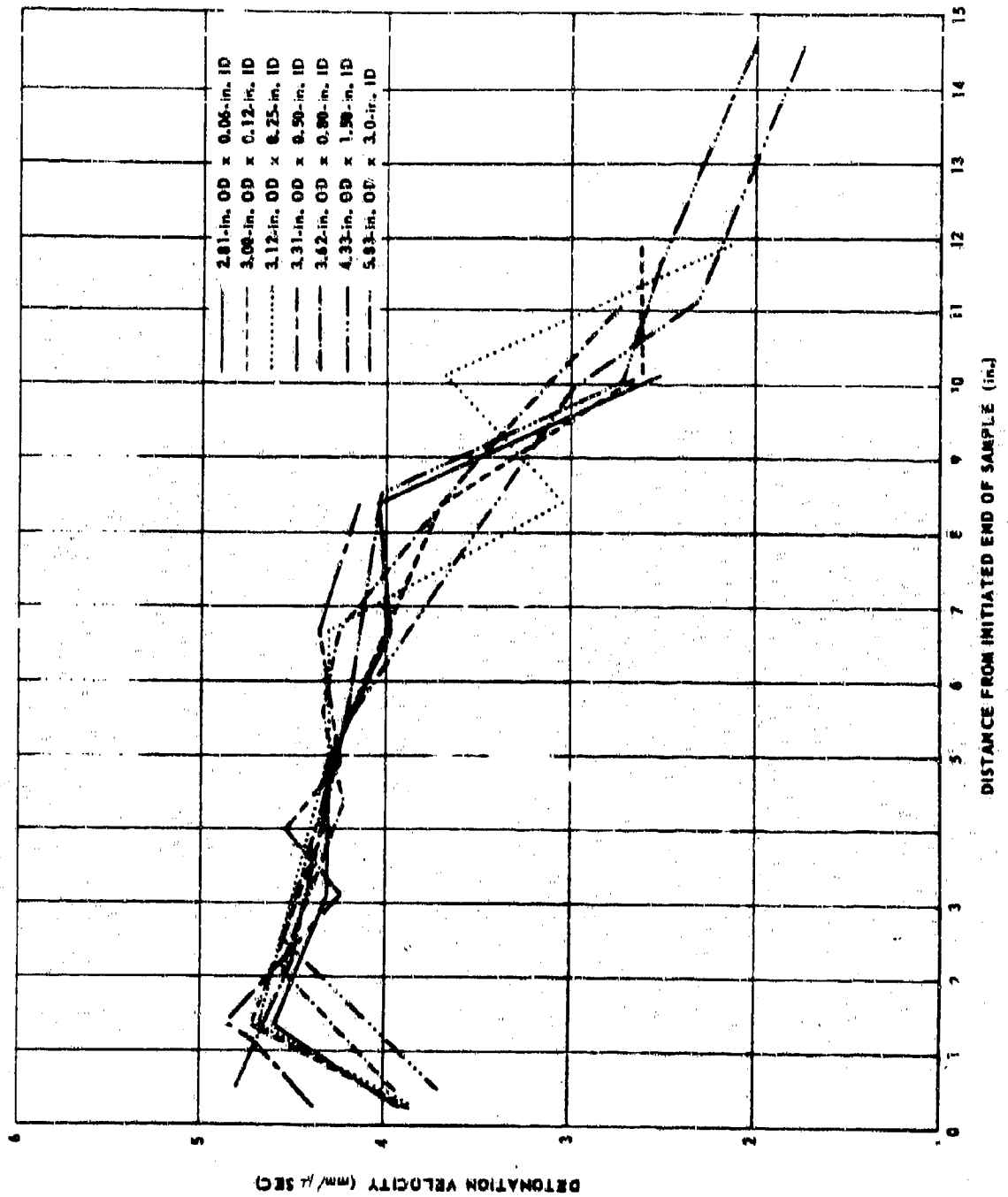

Figure 2. Detonation Velocity Behavior in 1.4-in. Web, Hollow Cylinders of AAB-3169. (Obtained at Points 1/4 into the Samples).

The results obtained at 1/2-web depth are shown in Figure 3 and are consistent with the preceding. The data indicate that from the middle of the web toward the outer surface of the hollow samples, the detonation wavefront is perpendicular to the charge axis until rapid fading begins.

The data obtained at the 3/4-web depth (Figure 4) are much more erratic than those from locations more removed from the inner surface. They also show no correlation with core size, but do indicate that fading begins somewhat sooner at this position, i.e., at 5 to 6 in.

The jet-velocity data (Figure 5) show some oscillatory behavior. More important, there is evidently a correlation between the size of the perforation and the velocity of the jet. It was observed that higher jet velocities occurred at smaller core sizes. This would be expected because the Mach interaction that produces the jet would be greatest when the core size is minimum.

Some experimental difficulty in probe placement, with the 0.06-in.-ID samples, prevented jet-velocity data from being obtained beyond the 4-in. distance. Probes further down the charge indicated low velocities more typical of the values obtained within the web, and these were assumed to have been owing to failure to reach the small core with the probes.

From these tests, it is concluded that the abortion of sustained detonation velocity is independent of core size over the 50-fold range from 0.06-in. to 3.0-in. ID.

3.1.4.2 Effect of Length

To determine whether the abortion of steady-state detonation is caused by an end-effect mechanism, it is necessary to test samples that vary in length. In the series of tests described in Section 3.1.4.1, samples having lengths equal to 4 times the OD were used. Since the web thickness was held constant, the OD varied in the same increments as the ID, and the lengths, therefore, varied over a two-fold range. Since no correlation was found between the location of the fadeout point and the ID, it follows that no correlation existed with the sample lengths either. However, a series of tests was planned explicitly to investigate the length effect using samples of identical cross-section (4.50-in. OD by 1.50-in. ID).

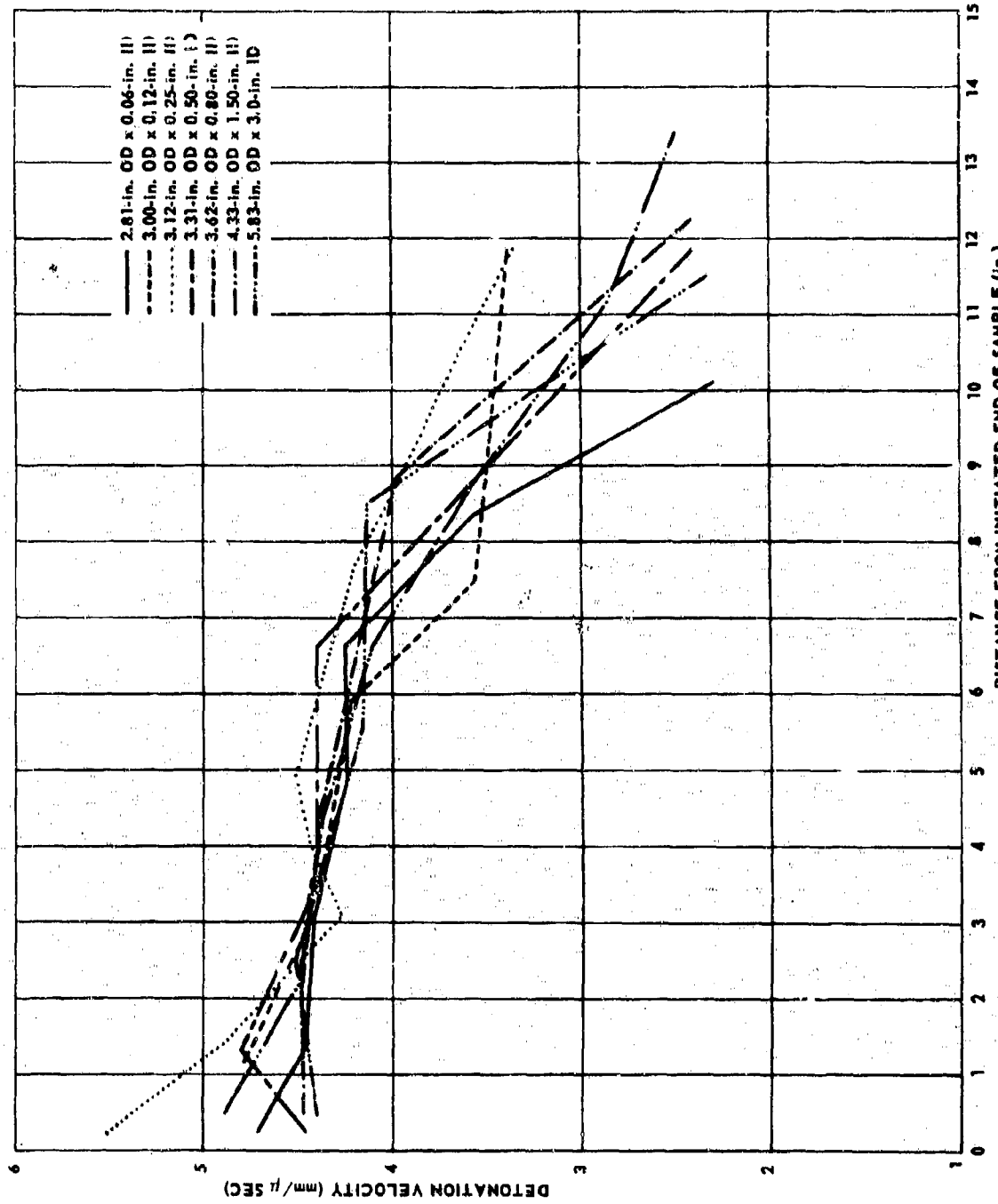

Figure 3. Detonation Velocity Behavior in 1.4-in. Web, Hollow Cylinders of AAB-3189. (Obtained at points 1/2 Web into the Samples).

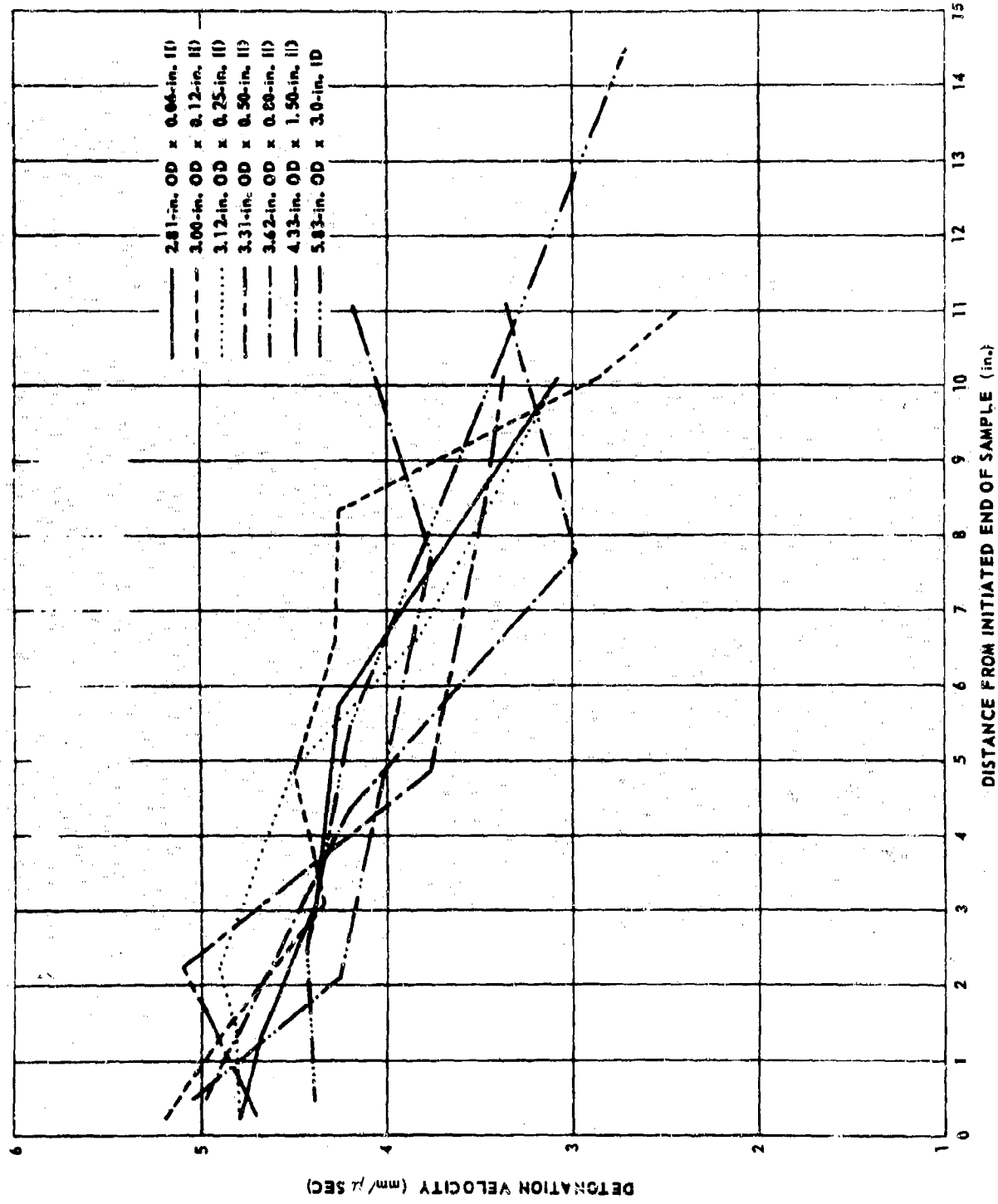

Figure 4. Detonation Behavior in 1.4-in. Web, Hollow Cylinders of AAB-3189. (Obtained at points 3/4-Web into the Samples)

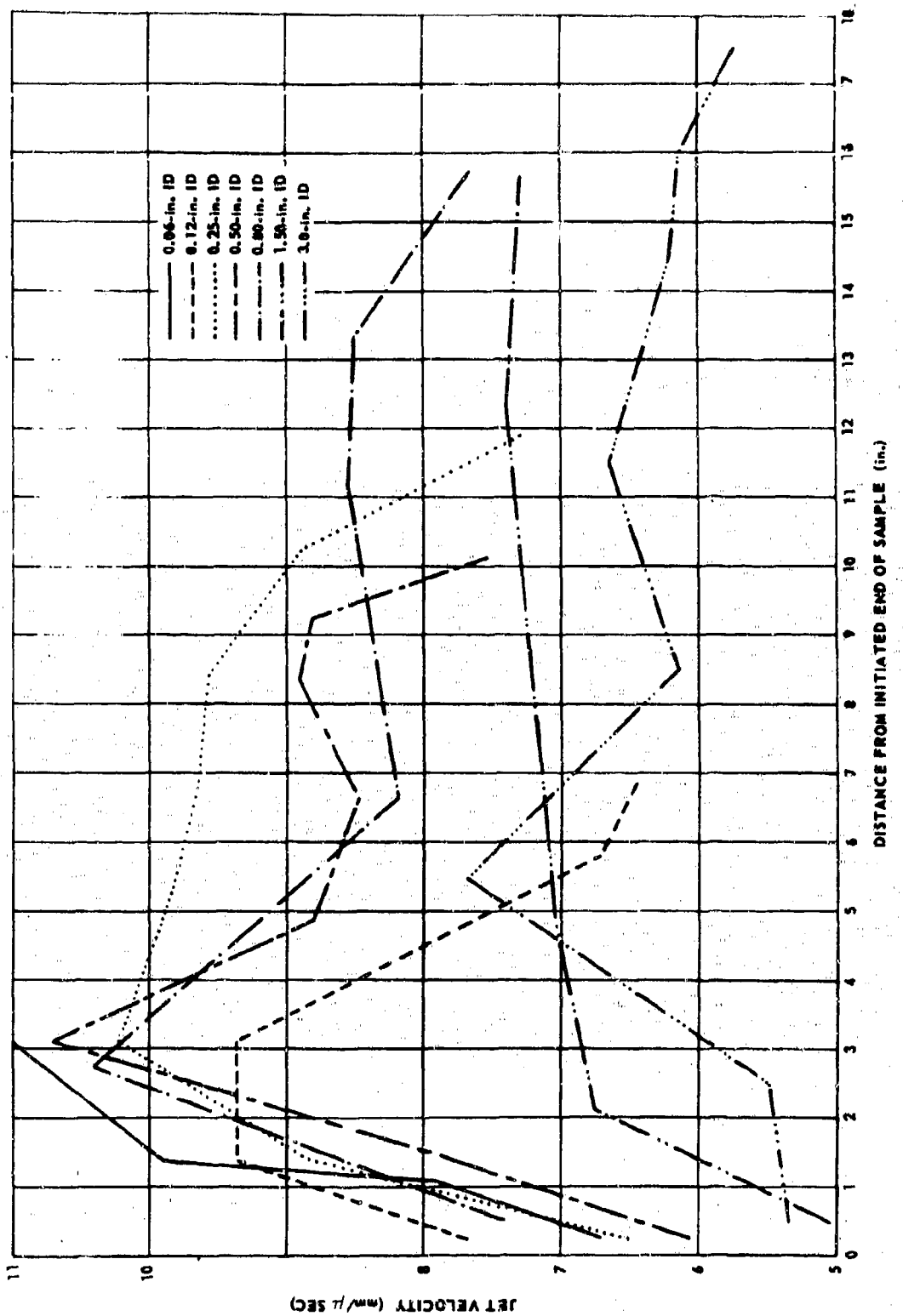

Figure 5. Jet Velocity in Hollow Cylinders of AAB-3189 Having 1.4 in. Web (Obtained at points on axis of sample).

Four sample lengths were tested: 18 in. (4 x OD), 22.5 in. (5 x OD), 27 in. (6 x OD), and 36 in. (8 x OD). The probe instrumentation was limited to two depths: one set inserted to 1/4-web thickness, the other to 3/4-web thickness. Plexiglas was used to attenuate the booster shock wave, for the same reasons discussed in Section 3.4.1.1.

Figure 6 shows the data obtained from the outer set of probes, reduced to detonation velocity vs distance along the sample. It is evident from these data that the sudden fading of the detonation velocity is not cuased by an end effect. The fading begins after approximately 24 in., and it is therefore not observed in the two smaller lengths. It should be noted in comparing the results for the 1.5-in. web to those obtained with the 1.4-in. web, that the 0.1-in. increase in web thickness extends the distance along the sample, through which a sustained detonation velocity occurs, from 7 to 24 in. This shows proof that, for a given material, the web size is the principal influence on the duration of a sustained detonation velocity, as judged by velocity data obtained near the outer surface of hollow samples.

Figure 7 reveals the extraordinary detonation-velocity data obtained from the inner set of probes. The velocities increased to near 7.5mm/μsec at the 24-in. distance. Again, the behavior of the detonation near the inner surface of hollow cylinders is seen to differ significantly from that near the outer surface. The outer portion of the web behaves more normally until the point is reached where the detonation fades. Since the inner portion is relatively more erratic, it is clear that a true steady-state sustained detonation occurs for only a short distance and this "detonation" is in fact a transient phenomenon.

3.1.4.3 Effect of Web Thickness

Two samples of AAB-3189 propellant were tested that measured 8-in. OD by 1.5-in. ID by 32-in. long. These were fired under the same conditions and with the same type of instrumentation as that shown in Figure 1. The data from the two tests were self-consistent. Figure 8 shows the velocity-vs-distance record of these tests and illustrates the behavior of detonation velocity in a hollow cylinder that has a web thickness (3.25 in.) that is much larger than the predicted pseudocritical web thickness (1.3 in.).*

*See Section 3.1.4.4 for a discussion of the critical geometry of hollow cylinders, and the definition of "pseudocritical."

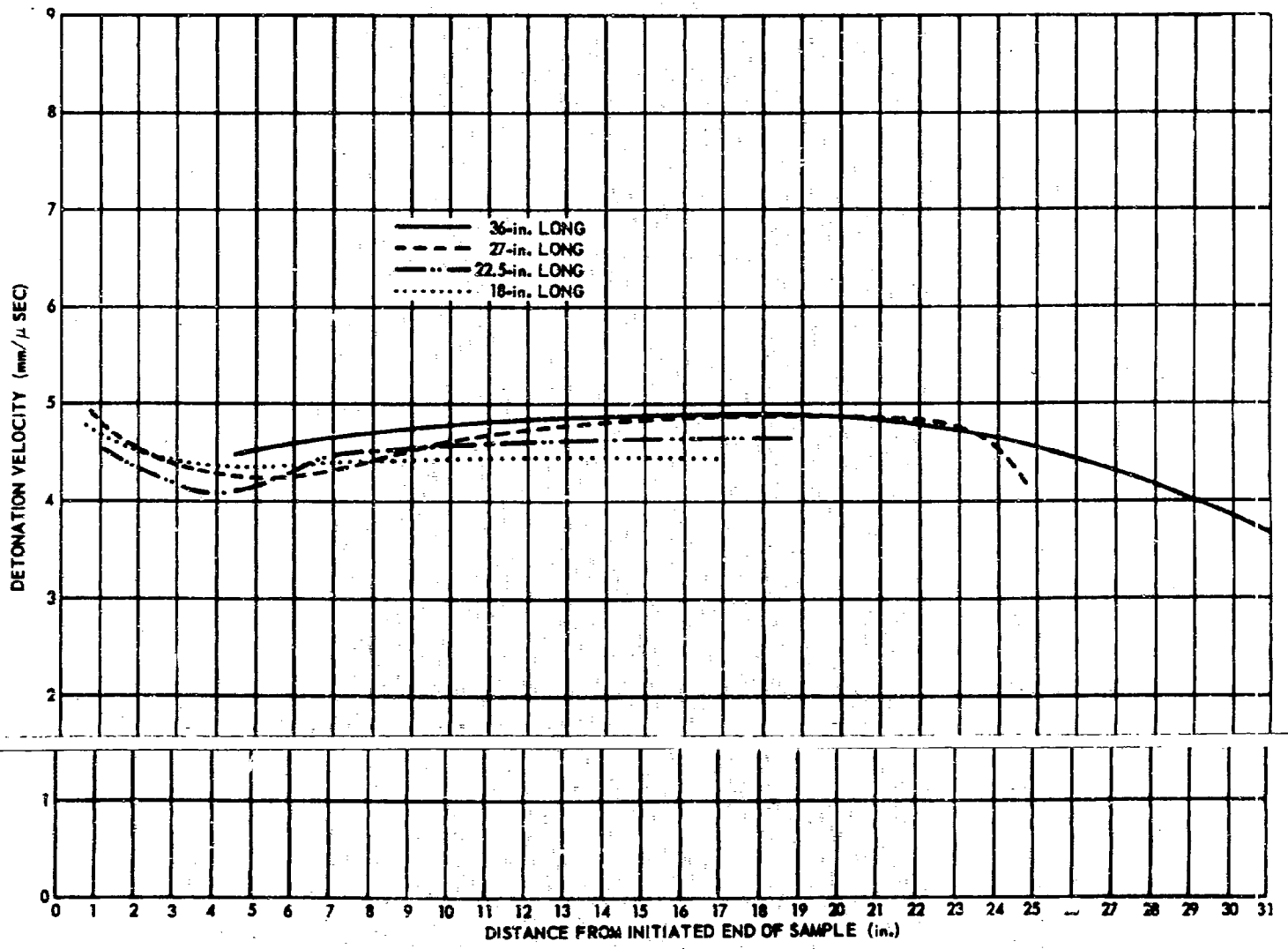

Figure 6. Detonation Velocity Behavior in 1.5-in. Web by 1.5-in. ID Hollow Cylinders of AAB-3189 (Obtained at points 1/4-Web into the sample).

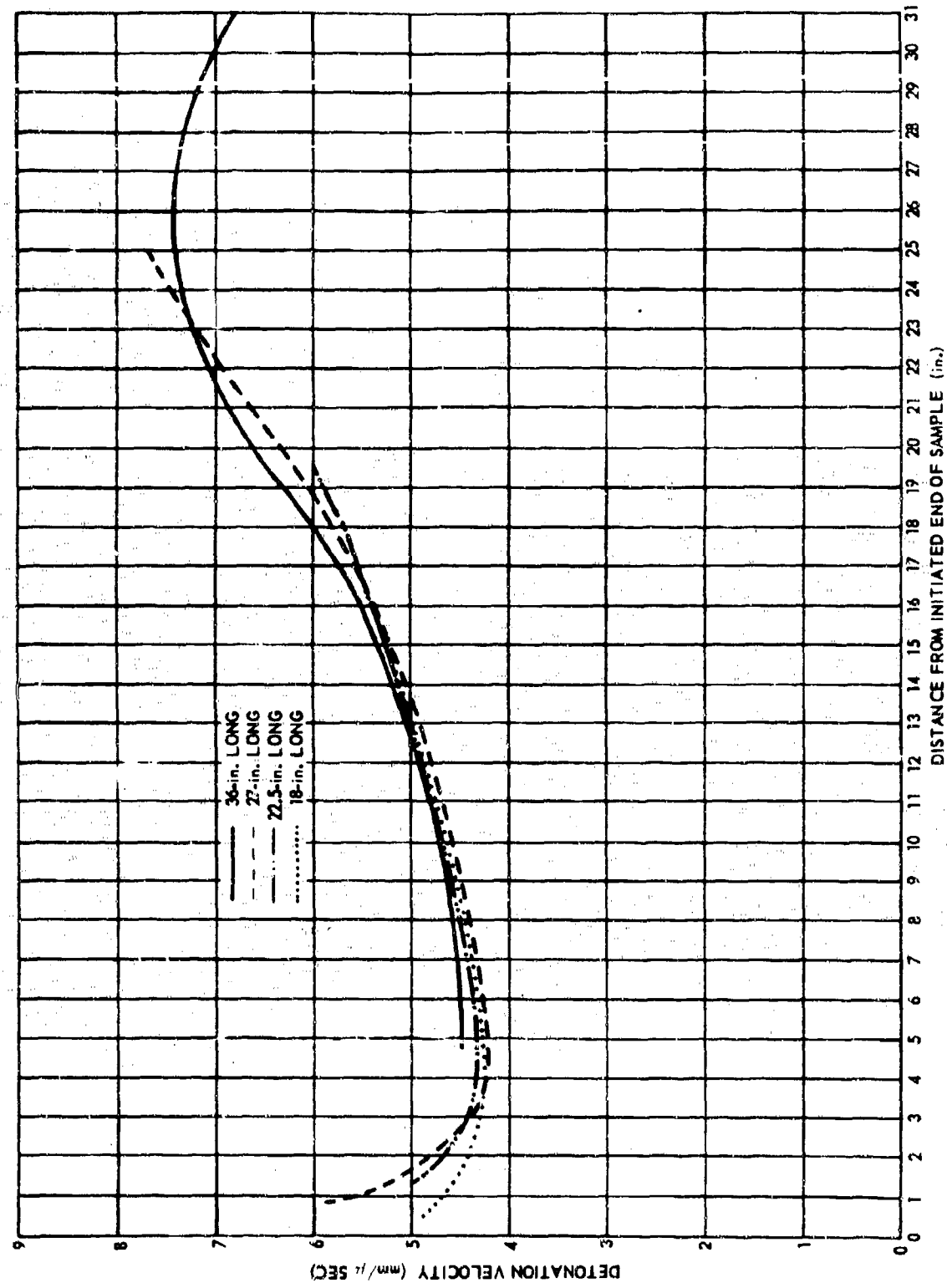

Figure 7. Detonation Velocity Behavior in 1.5-in. Web by 1.5-in. ID Hollow Cylinders of AAB-3189 (Obtained at points 3/4 web into sample).

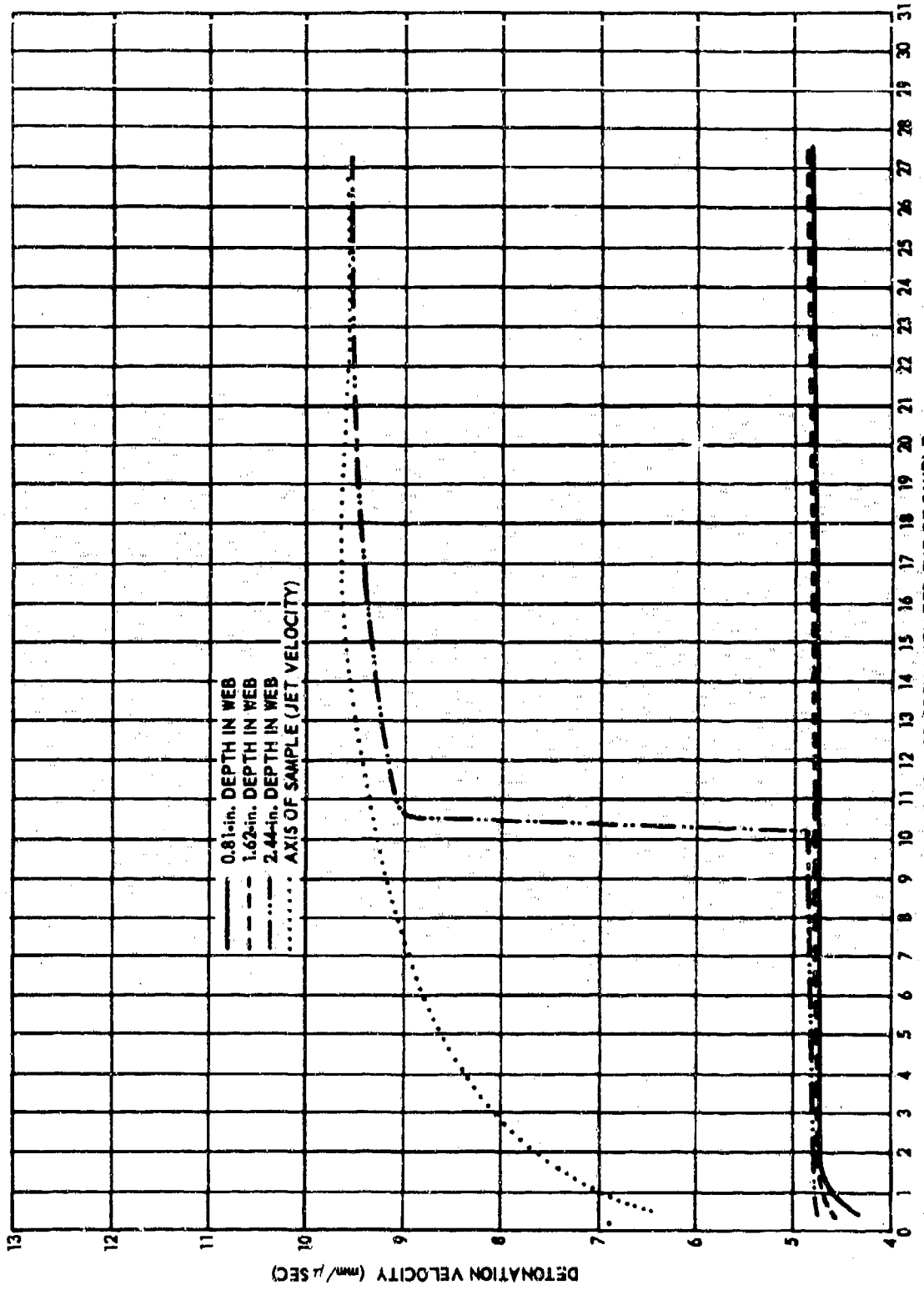

Figure 8. Detonation Velocity and Jet Velocity Behavior in 8-in. OD by 1.5-in. ID by 31-in. Long, Hollow Cylinder of AAB-3189.

Throughout the entire sample length the velocity of the wave over the outer half of the web remains constant (2.8 mm/μsec). At the 3/4-web depth, the same velocity is maintained for 10 in. and then the velocity increases very rapidly to reach an eventual maximum of 9.5 mm/μsec. The jet velocity increases to between 9.6 and 9.5 mm/μsec after 12.5 in.

Detonation of propellant at 9.5 mm/μsec is difficult to accept. Since this velocity agrees with the jet velocity, an alternative explanation for the high velocity registered by the 3/4-web probes can be postulated. Assume that the jet front causes ignition of propellant at the inner surface as it proceeds down the perforation. This is reasonable, because of the high temperature and high pressure characteristics of the jet. Assume further that, because of the high pressure in the perforation behind the jet front, the propellant will burn at a fast rate. It follows that, at a sufficient distance down the sample, enough time would elapse between the passage of the high-velocity igniting jet front and the arrival of the lower velocity reactive wave in the propellant to permit the burning propellant surface to reach the inner probes before the reactive wave in the propellant. Since the probes are triggered by shorting through a highly ionized medium, they could be triggered when the burning surface reaches them. The apparent velocity deduced from the inner (3/4-web) probes, from that point on, should be identical to the jet velocity, because the vector describing the regression of the burning inner surface in the longitudinal direction is equal to the velocity vector of the jet in the same direction (assuming a constant radial burning-rate vector).

Assuming this hypothesis to be true, the point where the burning surface first triggered the 3/4-web probes had been ignited 45 μsec earlier by the jet front. For 0.8 in. of propellant to burn in 45 μsec requires an average burning rate of 0.45 mm/μsec. No propellant burning-rate data have been measured near this rate. Extrapolation of the ammonium perchlorate burning-rate expressions developed in Reference 5 yields an estimate of the pressure required to cause burning at 0.45 mm/μsec. This pressure estimate is between 5 and 100 kbar, using these equations respectively:

$$B = 0.70 \sinh (1.59 \times 10^{-4} P) \qquad (17)$$

and

$$B = 2.0 \times 10^{-7} P^{1.75} \qquad (18)$$

where B is the burning rate (in./sec) at pressure P (psig). Since Equation 17 fits the data better at the higher pressure range, it may be inferred that the required pressure is nearer the 5-kbar level. No measurement of the static pressure within a cylindrical jet cavity exists, so there is no way to determine the probability that such high burning rates are possible.

3.1.4.4 Conclusions

Based on the reported findings of the jetting phenomena test series, the following conclusions are made. By all considerations, these conclusions are subject to revision and correction pending further study of this complex problem.

a. Core diameter does not affect the abnormal behavior of the detonation wave in hollow cylindrical samples.

b. The abnormal behavior of the detonation wave is not caused by an end-effect mechanism.

c. The principal cause for abnormal behavior of the detonation process in hollow cylindrical samples is the web thickness; specifically, the size of the web that exceeds a pseudocritical value, which is defined as that size below which no transitory sustainment occurs.

d. The mechanism that causes abnormal quenching of the detonation process consists of a radial burning, directed outward from the inner surface, which proceeds at a high rate and reduces the web size to below the pseudocritical value.

The last conclusion expresses the present interpretation of the test results, which does not consider any other perturbation to steady-state behavior than the high burning rate process. If such a process can continue unabated, clearly no classically supercritical hollow cylinder is possible. However, the duration of high pressure at a fixed distance down the sample must certainly be finite, because the jet slug must have finite length. Therefore it is possible that a hollow-core sample could be made having a web sufficiently larger than the pseudocritical size to remain supercritical after the limited burning process has consumed a portion of the inner web surface.

The entire jetting problem is not well enough understood in its basic fundamentals to allow further speculation about this and other possibilities. The primary question that remains unanswered is how a jet, traveling at about twice the velocity of a detonation reaction in the web of a hollow sample, continues to receive energy from that reaction despite the continuously increasing separation of the two fronts. If the jet velocity exceeds the detonation-wave velocity, steady-state conditions would be impossible in hollow-core samples. This fact alone rules out discussion of critical size and supercritical size, when speaking of the hollow cylinder. These terms need to be modified, by using the prefix "pseudo." Thus, pseudocritical geometry is defined as the minimum geometry in which detonation can be sustained for a minimal distance, and pseudosupercritical geometry is defined as any geometry larger than the pseudocritical geometry. This convention has been adopted in Section 3.2.1.3, where the critical geometry subtask considers hollow cylinders.

3.2 TECHNICAL DISCUSSION - PHASE 2 SUBTASKS

3.2.1 Critical Geometry (Subtask 3.3.2)

3.2.1.1 Equilateral Triangle

AAB-3189 propellant from Batch 4EH-108 was cast into 30 equilateral triangular cross-section columns for testing to determine the critical geometry of this shape. Five samples were to be cast at each of the following nominal sizes: 4.05, 4.15, 4.25, 4.35, 4.45, and 4.55-in. Modifications to the molds before the casting took place raised each of the sets of dimensions by approximately 0.20 in., which produced a series of samples ranging from 4.25- to 4.75-in. All the columns had a length-to-side ratio of 4.

By the theory of critical geometry for the equilateral triangular column

$$\sigma_c = \frac{b_c}{\sqrt{3}} \qquad (19)$$

where σ_c is the critical geometry and b_c is the critical length of a side of the triangle.

From the results of 21 tests performed with these samples (Table 3 and Figure 9), the maximum likelihood estimate of the mean critical side is 4.50-in. The critical geometry, by Equation 19, is 2.60 in. Batch-control tests showed the critical diameter of Batch 4EH-108 to be equal to 2.73 in. Further analyses of these results and those obtained with the other shapes is given in Section 3.2.1.4.

3.2.1.2 Rectangle

Eighteen critical-geometry tests were conducted using rectangular cross-section samples. The samples were cast from AAB-3189 propellant in Batch 4EH-110, which had a critical diameter of 2.92 in. As in all the critical-geometry tests of solid shapes, the explosive booster cross-section was identical to that of the acceptor.

Since the rectangle is a two-parameter shape, for these tests it was decided to keep the thickness constant and vary only the width of the samples. The critical geometry is less sensitive to incremental changes in width than it is to the same changes in thickness. This is evident by inspection of the defining equation:

$$\sigma_c = \left(\frac{2wt}{w + t} \right)_c \tag{20}$$

where w is the width and t is the thickness of the rectangle. Since t was chosen to be 1.75-in., Equation 20 may be written

$$\sigma_c = \frac{3.5\, w_c}{1.75 + w_c} \tag{21}$$

for this particular series of tests.

The test results are given in Table 4. The maximum likelihood estimates of the mean critical width and the standard deviation are 6.31 and 0.26 in., respectively. By Equation 21, the critical geometry for these rectangles is 2.74 in.

Table 3. Test Results, Subtask 3.3.2, Equilateral Triangles.

Triangle Side		Density (gm/cc)	Result of Test	Average Detonation Velocity (mm/μsec)	Test No.
Mean (in.)	Standard Deviation (in.)				
4.25	0.061	1.732	No-go	--	3.3.2.2
4.35	0.027	1.733	No-go	--	3.3.2.3
4.35	0.047	1.730	No-go	--	3.3.2.8
4.35	0.049	1.729	No-go	--	3.3.2.9
4.37	0.036	1.731	No-go	--	3.3.2.10
4.38	0.030	1.729	No-go	--	3.3.2.11
4.47	0.043	1.730	No-go	--	3.3.2.12
4.48	0.039	1.732	No-go	--	3.3.2.13
4.49	0.038	1.730	No-go	--	3.3.2.4
4.50	0.060	1.734	Go	4.24	3.3.2.1
4.50	0.069	1.731	Go	4.25	3.3.2.5
4.50	0.054	1.731	No-go	--	3.3.2.15
4.54	0.038	1.729	Go	4.32	3.3.2.6
4.54	0.032	1.728	Go	4.26	3.3.2.16
4.56	0.045	1.731	Go	4.30	3.3.2.7
4.56	0.061	1.730	Go	4.29	3.3.2.14
4.64	0.025	1.728	Go	4.34	3.3.2.21
4.67	0.054	1.730	Go	4.31	3.3.2.20
4.67	0.065	1.727	Go	4.32	3.3.2.18
4.70	0.070	1.729	Go	No data	3.3.2.19
4.75	0.052	1.729	Go	4.41	3.3.2.17

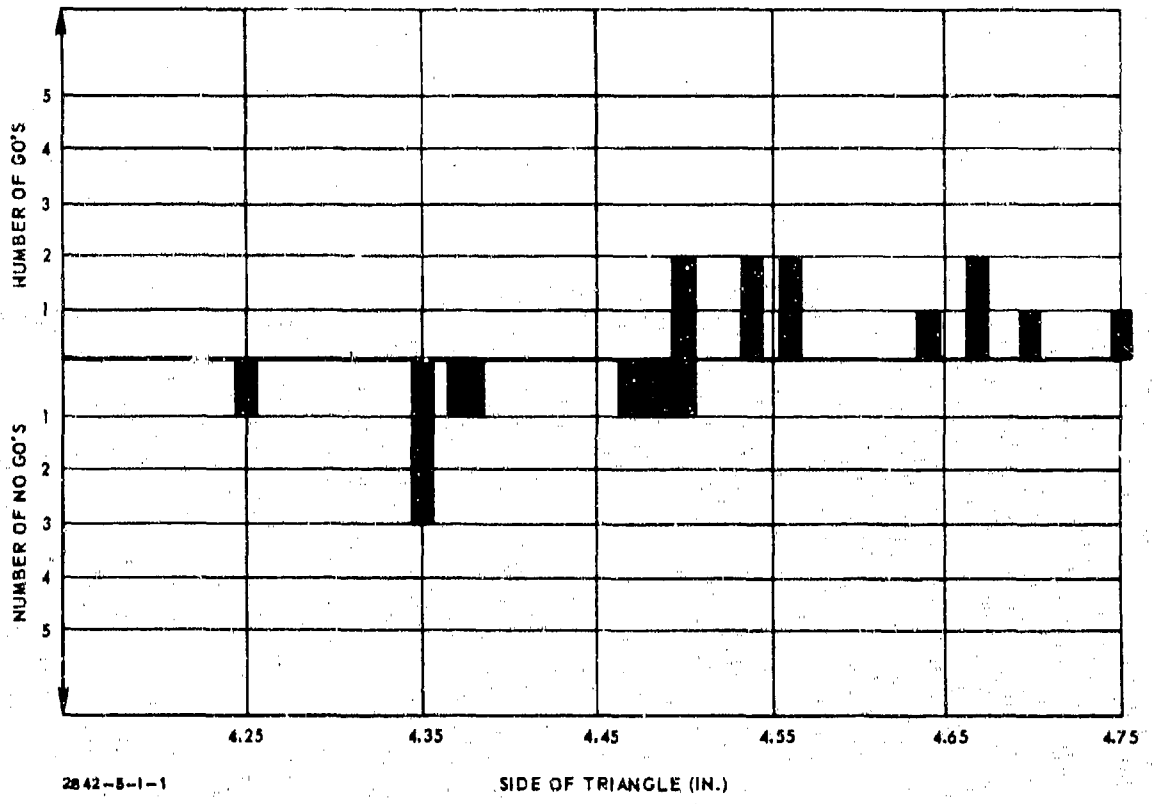

Figure 9. Go - No Go Results, Batch 4EH-108 Equilateral Triangles, AAB-3189.

Table 4. Test Results for Rectangular Slabs (AAB-3189) 1.75 in. Thick by 11.75 in. Long.

Width (in.)	Result	Average Detonation Velocity (mm/μsec)	Test No.
5.00	No-go	--	3.3.2.78
5.75*	No-go	--	3.3.2.77
5.75	No-go	--	3.3.2.49
5.875	No-go	--	3.3.2.50
5.875	No-go	--	3.3.2.51
6.00	No-go	--	3.3.2.48
6.00	No-go	--	3.3.2.42
6.00	Go	4.19	3.3.2.37
6.125	No-go	--	3.3.2.46
6.125	No-go	--	3.3.2.47
6.25	No-go	--	3.3.2.45
6.50	Go	4.38	3.3.2.44
7.00	Go	4.24	3.3.2.43
7.75	Go	4.29	3.3.2.41
9.00	Go	4.29	3.3.2.38
9.50	Go	4.13	3.3.2.40
10.00	Go	4.26	3.3.2.39
11.75	Go	4.31	3.3.2.35

*Sample length = 23.5 in.
Average density = 1.726 gm/cc

3.2.1.3 Hollow Cylinders

Critical-geometry tests have been conducted on circular-core and cross-core hollow cylinders. A series of tests for both of these shapes was performed using perforations of two different sizes. Variation of the sample sizes within each set was controlled by the OD of the samples.

The interpretation of the critical-geometry tests for hollow cylinders is different from that employed for all other shapes tested. The discussion of jetting phenomena (Section 3.1.4) explains the reasons for this difference. Since the critical-geometry theory was developed as a first-order approximation that did not consider interactions, to evaluate the theory as it stands requires determination of the pseudocritical geometry for hollow cylinders. The definition of this term previously given is the minimum geometry below which no sustained detonation can occur over a finite distance.

Determination of the pseudocritical size is accomplished by reducing distance-vs-time data obtained from probes placed in the samples to a depth equal to 1/2-web thickness. The distance over which a sustained detonation occurs is determined from the data for those sizes in which this behavior is observed. An estimation of the pseudocritical size could be made from the assembled data on propagation distance vs sample size by assuming a linear relationship and extrapolating a best-fit line to zero propagation distance. Considering the difficulty involved in obtaining an accurate propagation distance estimate, however, and noting the high sensitivity of propagation distance to web size (Section 3.1.4.2), it is more proper to consider that the size at which propagation occurs for approximately two web thicknesses is a reasonable estimate of the pseudocritical size.

The results of the circular-core tests are shown in Table 5. The critical diameter of Batch 4EH-109 material from which these were cast is 2.92-in. By the critical-geometry theory, the pseudocritical geometry of a circular-core hollow cylinder is equal to the difference between the OD and the ID of the pseudocritical sample.

For the 1.5-in.-ID samples, the pseudocritical size is 4.12 in. OD, which corresponds to a pseudocritical geometry of 2.62 in. The pseudocritical size of the 3-in.-ID samples is 5.62 in. OD, which also yields 2.62 in. as the pseudocritical geometry.

Table 5. Test Results, Subtask 3.3.2, Circular-Core Hollow Cylinders AAB-3189.

ID (in.)	OD (in.)	Propagation Distance (in.)	Detonation Velocity (mm/μsec)	Test No.
1.5	4.25	13	4.29	3.3.2.28
	4.25	17	4.32	3.3.2.69
	4.12	2.5	4.23	3.3.2.29
	4.12	4	4.28	3.3.2.70
	4.00	0	--	3.3.2.30
	4.00	0	--	3.3.2.71
	3.88	0	--	3.3.2.31
	3.88	0	--	3.3.2.72
	3.75	0	--	3.3.2.32
	3.75	0	--	3.3.2.73
	3.62	0	--	3.3.2.33
1.5	3.62	0	--	3.3.2.74
3.0	5.75	7	4.23	3.3.2.22
3.0	5.75	8.5	4.28	3.3.2.56
	5.62	4.5	4.22	3.3.2.23
	5.62	5	4.25	3.3.2.75
	5.50	0	--	3.3.2.24
	5.50	0	--	3.3.2.55
	5.38	0	--	3.3.2.25
	5.38	0	--	3.3.2.54
	5.25	0	--	3.3.2.26
	5.25	0	--	3.3.2.36
	5.25	0	--	3.3 2.53
	5.12	0	--	3.3.2.27
3.0	5.12	0	--	3.3.2.52

The results of tests that involved cross-core pe rforations are shown in Table 6. The cross-shape perforation is cor nposed of four square arms of equal dimensions. By the critical-geo metry theory,

$$\sigma_c = \frac{(OD)_c^2 - 20\ell^2}{(OD)_c + 12\ell} \qquad (22)$$

where σ_c is the pseudocritical geometry and (O $)_c$ is the pseudocritical outer diameter of a sample perforated by a "sq are" cross of which the width (and length) of each arm is equal to ℓ a constant.

When ℓ equals 0.5 in., the pseudocritical OD i s 4.12 in., which (by Equation 22, gives a pseudocritical geometry o f 2.56 in. For ℓ equal to 1.0 in., the pseudocritical OD is 5.50 in., whi ch also yields a value of 2.56 in. for the pseudocritical geometry.

3.2.1.4 Conclusions

A summary of the analyzed critical-geometry r esults is given in Table 7, which shows the calculated critical an d pseudocritical geometries for square, triangular, and rectang ular columns, and hollow-core cylindrical shapes, compared with the critical diameters of the batches from which the samples were ca t.

Two attempts to find a correlation between the critical diameter and critical geometry for all shapes are shown in T able 7. The difference between critical diameter and critical geometr y does not provide a good correlation among the shapes. Correlation in terms of differences does not have a strong physical justification eit her.

The ratio of critical geometry to critical diam ter for each shape is more uniform and represents a plausible me ans of correlating the critical-geometry data. Since all the tests in this subtask used AAB-3189 propellant, any attempt to make gen eral conclusions regarding the critical-geometry theory would be premature. The verification tests (Subtask 3.3.3) using AAB-32 25 propellant will provide data that will facilitate the determinati on of a proper correlation method.

Table 6. Test Results, Subtask 3.3.2, Cross-Core Hollow Cylinders AAB-3189.

Width and Length* (in.)	OD (in.)	Propagation Distance (in.)	Detonation Velocity (mm/μsec)	Test No.
0.5	4.25	8.5	4.33	3.3.2.66
	4.12	8	4.23	3.3.2.64
	4.00	0	--	3.3.2.63
	3.88	0	--	3.3.2.67
	3.75	0	--	3.3.2.65
0.5	3.62	0	--	3.3.2.68
1.0	5.75	8.5	4.35	3.3.2.62
	5.62	8.5	4.28	3.3.2.61
	5.50	6	4.29	3.3.2.60
	5.38	0	--	3.3.2.34
	5.25	0	--	3.3.2.58
1.0	5.12	0	--	3.3.2.57

*

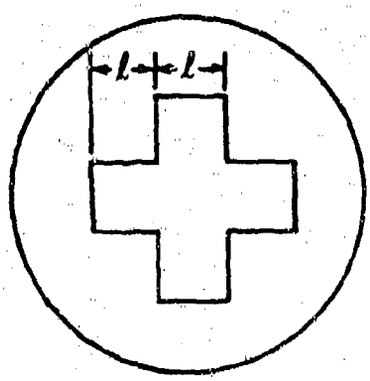

Table 7. Critical and Pseudocritical Geometries for Various Shapes, AAB-3189.

Shape	Critical Geometry, σ_c (in.)	Batch Critical Diameter, d_c (in.)	$d_c - \sigma_c$	σ_c / d_c
Square	2.49	2.71	0.22	0.92
Equilateral Triangle	2.60	2.73	0.13	0.95
Rectangle	2.74	2.92	0.18	0.94
Circular-Core Hollow Cylinder	2.62*	2.97	0.35	0.88
Cross-Core Hollow Cylinder	2.56*	2.92	0.36	0.88

Mean $(\sigma_c / d_c) = 0.92$

Standard Deviation = 0.03

*Pseudocritical geometry

The jetting phenomenon, which perturbs the detonation of hollow cylinders in the sizes used in this test program, has been discussed (Section 3.1.4). To make any conclusions for a large, full-scale rocket motor having a core size of 2 to 3 ft is still a tenuous proposition because there has been no experimental work performed to establish the length of time it would take for a jet to form or if it would form at all in a core of this size. Should the jet be sufficiently delayed, or nonexistent, in a large-core grain, there might exist a true critical size. In other words, the introduction of the "pseudocritical" concept to the critical-geometry theory may be necessary only when describing the behavior of relatively small ID grains. This important point strongly suggests the need for large-scale critical-geometry tests to resolve the questions regarding applicability of the theory to large motor systems.

3.2.2 Verification of Theory (Subtask 3.3.3)

The purpose of this subtask is to determine the applicability of the critical geometry theory to a material different from AAB-3189. The propellant to be used is AAB-3225, which has 7.1% RDX substituted for an equal weight of ammonium perchlorate. The sample shapes to be tested are square columns and perforated cylinders; the latter to include two sizes of circular cores and two sizes of cross-cores.

The molds are at the Sacramento Plant awaiting the casting operation. Sizes were selected according to a statistical design that will place all the testing at approximately $\pm$ 3 standard deviations from the estimated mean critical geometry, which is predicted by multiplying the critical diameter of AAB-3225 by the ratio of critical geometry to critical diameter determined from the AAB-3189 tests (Table 7). The sample sizes are given in Table 8. If the theory is correct, the larger samples of any set should all be supercritical (or pseudosupercritical in the case of the hollow samples) and the smaller samples of each set should be subcritical. The present schedule calls for testing these samples in January 1967.

3.2.3 Initiation Pressure vs Pulse Width (Subtask 3.3.4)

A calculation was made to estimate the velocity and thickness of an aluminum plate that would be sufficient to initiate detonation in a 4-in.-diameter sample of AAB-3189 propellant. Based on this calculation, preliminary tests will be conducted with 1/8-in.-thick and 1/4-in.-thick

Table 8. Sample Sizes for Verification Tests, AAB-3225.

Square Columns			Circular-Core Cylinders				Cross-Core Cylinders*			
No.	Size of Sq (in.)	Height (in.)	No.	OD (in.)	ID (in.)	Height (in.)	No.	OD (in.)	Cross (in.)	Height (in.)
4 each	4-1/2	25	4 each	7-1/4	3	36	4 each	7-1/4	3 (ℓ = 1 in.)	36
4 each	5-1/8	25	4 each	8	3	36	4 each	8	3 (ℓ = 1 in.)	36
			4 each	10-1/4	6	48	4 each	10-1/4	6 (ℓ = 2 in.)	48
			4 each	11	6	48	4 each	11	6 (ℓ = 2 in.)	48

*

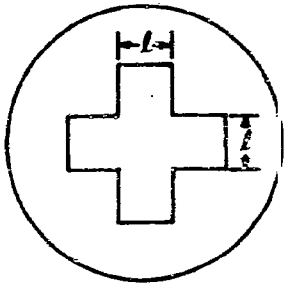

aluminum plates projected to 3500 fps. This set of conditions should produce, in both cases, a 49.1 kbar shock pressure in the propellant. The pulse widths should be 4.0 mm for the 1/8-in. plate and 8.0 mm for the 1/4-in. plate. The event will be photographed using the 100 kv X-ray facility available at Aerojet's Chino Hills Ordnance Laboratory.

3.2.4 Initiation Pressure vs Diameter (Subtask 3.3.5)

Through a redirection of the technical effort, this subtask has been enlarged to consist of tests to determine the initiation criteria for AAB-3189 (9.2% RDX), AAB-3225 (7.1% RDX), and AAB-3267 (5% RDX) propellants. The objective is to use these data to estimate the initiation criterion for unadulterated propellant (ANB-3226).

Sensitivity investigations were conducted under AF 04(611)-9945 with AAB-3189 propellant to a diameter of 6 in. (Reference 4). From this study, the Hugoniot of AAB-3189 is available. The Hugoniots of the other two formulations must be determined in the current program. Also required are additional data on the attenuation of a shock wave in large Plexiglas columns. These two efforts, plus the card-gap sensitivity tests themselves, comprise this subtask.

3.2.4.1 Hugoniot Determination

The method used to determine the Hugoniot of propellant is identical to that described in Reference 4. The charge is prepared by alternately stacking 1/4-in.-thick by 1-in.-diameter Plexiglas discs and 0.08-in. thick by 1-in.-diameter propellant wafers to form a column approximately 1-1/2-in. high. The column is shocked with a Composition B cylindrical booster, 1 in. in diameter by 2 in. high. The column is backlighted with an Argon bomb and the event is recorded on a Beckman and Whitley streak camera. From the streak record, velocities in the Plexiglas are determined at each Plexiglas-propellant interface.* Average velocities in the propellant are determined by dividing the propellant thickness by the time difference between the moment the shock enters the wafer and the moment it emerges at the propellant-Plexiglas interface.

---

* The custom in identifying interfaces is to first name the material from which the shock passes, and second name the material into which the shock is transmitted.

The streak record thus furnishes data from which the incident-shock velocity U_i in Plexiglas and the average transmitted shock velocity U_t in propellant are calculated.

The following Hugoniot of Plexiglas, used in the subsequent calculations, was reported in Reference 6:

$$P = 5.51\,U^2 - 14.03\,U \tag{23}$$

where P is the shock pressure in kbar, and U is the shock velocity in mm/μsec. This equation can be written:

$$P = 30.25\,\mu + 21.56\,\mu^2 \tag{24}$$

where μ is the particle velocity in mm/μsec by using the relationships:

$$P = 10\,\rho_o\,U\mu \text{ and } \rho_o = 1.188 \text{ gm/cm}^3.$$

A point on the P(μ) propellant Hugoniot is obtained by solving these two equations:

$$P = 10\,\rho_{o,2}\,\bar{U}_t\,\mu \tag{25}$$

and

$$P = 21.56\,(2\,\mu_i - \mu)^2 + 30.25\,(2\,\mu_i - \mu) \tag{26}$$

where $\rho_{o,2}$ is the density of the propellant and μ_i is the incident particle velocity in Plexiglas corresponding to $\bar{U}_i$. Equation 26 is a "reflection" of the P(μ) Plexiglas Hugoniot about $\mu = \mu_i$.

a. AAB-3189 Propellant Hugoniot

In the current program, the reflection operation was performed graphically, whereas under Contract AF 04(611)-9945 it was performed analytically. By graphical reflection, the Hugoniot for AAB-3189 was found to be:

$$P = 33.27\,\mu + 44.45\,\mu^2$$

or

$$P = 6.694\,U^2 - 12.913U$$

By mathematical reflection, using the same data generated on SOPHY I, the Hugoniot for AAB-3189 becomes:

$$P = 32.18\,\mu + 47.80\,\mu^2 \qquad (29)$$

or

$$P = 6.225\,U^2 - 11.613U \qquad (30)$$

The revised Hugoniot does not significantly alter the initiation criterion reported in Reference 4. Pressure values calculated with the revised Hugoniot differ from the reported data only in fractions of one kilobar.

b. AAB-3225 Propellant Hugoniot

Table 9 shows the values of U_i and U_t calculated from the streak records of two Hugoniot tests, the corresponding shock pressure and particle velocities calculated from the Plexiglas Hugoniot, and the shock pressures and particle velocities computed for AAB-3225 by Hugoniot-reflection. The best-fit quadratic to the computed Hugoniot points is:

$$P = 27.38\,\mu + 62.75\,\mu^2 \qquad (31)$$

or

$$P = 4.797\,U^2 - 7.570U \qquad (32)$$

Equation 31 is shown graphically in Figure 10 with the data points from which the equation was derived.

c. AAB-3267 Propellant Hugoniot

Hugoniot determinations on AAB-3267 propellant will be made in January 1967, as soon as cured samples become available from the casting line at the Sacramento Plant.

3.2.4.2 Plexiglas Attenuation of Shock Waves

The sizes of the samples that will be tested by the card-gap techniques (Section 3.2.4.3) are much larger than any other samples that have been tested this way. To determine the initiation criterion for each propellant formulation by the card-gap method, it is necessary that the

Table 9. Hugoniot Data for Test AAB-3225.

Measured	Calculated		Measured	Calculated	
U_i (mm/μsec)	P_i (kbar)	μ_i (mm/μsec)	U_t (mm/μsec)	P_t (kbar)	μ_t (mm/μsec)
4.85	62	1.07	5.08	75	0.85
4.66	54	0.98	4.14	61	0.84
4.23	39	0.78	4.17	46	0.64
3.84	27	0.60	3.29	30	0.53
3.63	22	0.50	3.02	24	0.45
3.30	14	0.35	2.71	15	0.31
3.02	8	0.22	2.68	9	0.19

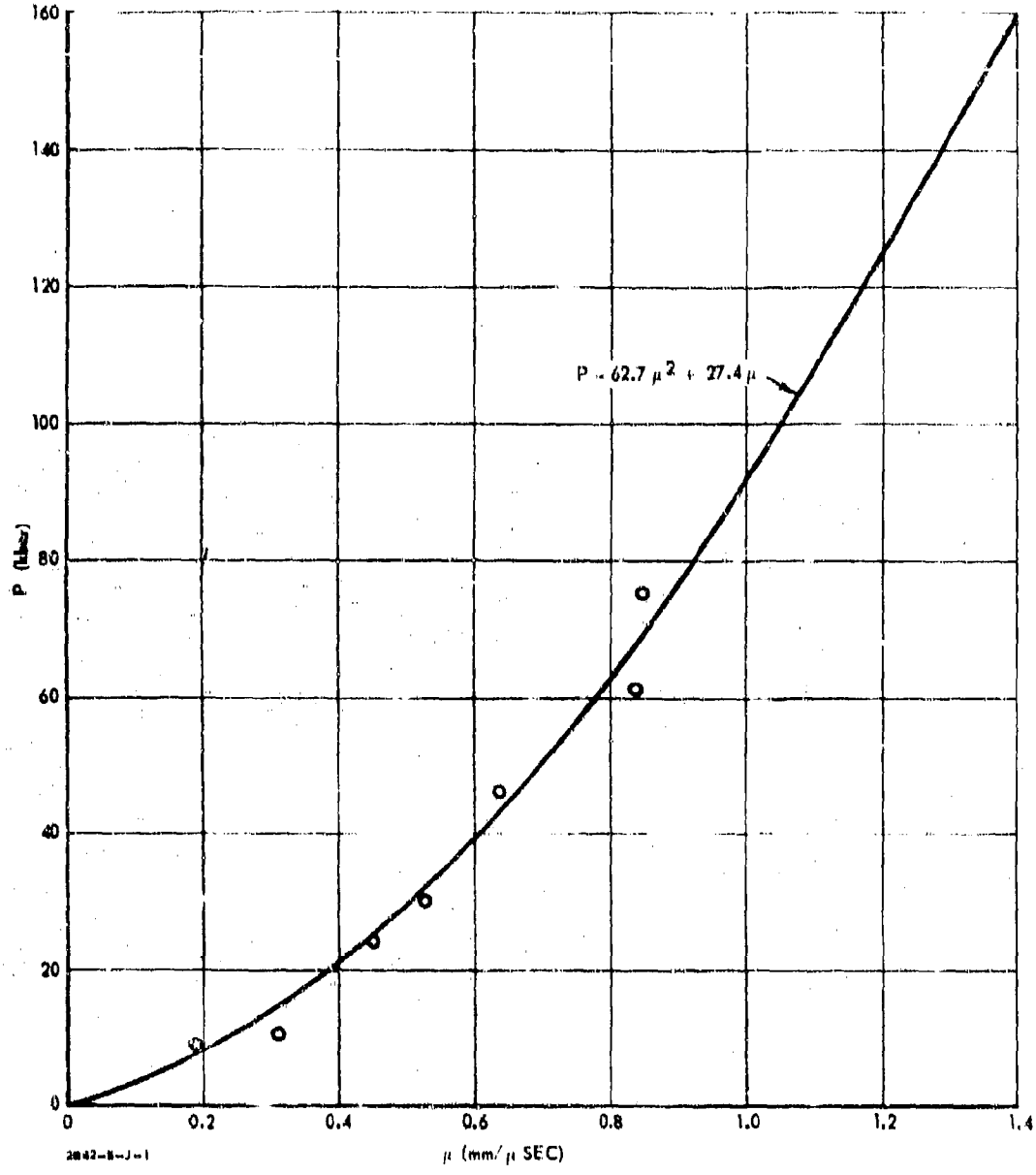

Figure 10. Hugoniot for AAB-3225.

incident shock pressure at the Plexiglas-propellant interface be known. To gather the information requires either the direct measurement of incident velocity for each test (by photographic or electrical means) or the determination of a shock velocity vs distance curve for each size Plexiglas column. The former is an extremely difficult experimental task when performed. Therefore, attenuation data will be gathered from a stacked column of 1-in.-thick Plexiglas plates. The stacked plates are required because of the unavailability and high cost of solid rods at the diameters demanded by this test series.

The photographic records from several tests with 8-in.-square plates were consistently poor in one respect. The shock wave location was obscured near each Plexiglas interface and in some cases there appeared to be severe distortion caused by the laminar column. Since the data were so inadequate for use in determining an attenuation curve, another approach had to be initiated. This approach used ionization probes to determine times-of-arrival of the shock wave at various distances down the column.

Initially, several arrival times were obtained from preliminary card-gap tests in which the trigger probe was placed at the booster-Plexiglas interface and the next probe was placed at the Plexiglas-propellant interface. To obtain velocity-attenuation data over the whole column, it is necessary to probe many interfaces within the column.

Tests will soon be conducted in which sets of two 30-gage enameled copper wires will be placed at various interfaces within stacks of 8-in. square, 9-in. square, etc., Plexiglas plates. These wire probes will be connected through a mixer box to a rasteroscillograph that will record distance-time data. Preliminary evaluation of the use of this type of probe has proven it successful. It remains to be seen whether a large number of such probes will seriously perturb the shock wave attenuation rate.

3.2.4.3 Card-Gap Sensitivity Tests

Molds have been fabricated and the propellant and booster casting schedules established to prepare samples for the extended effort in this subtask. The minimum initiating shock pressure will be determined for AAB-3189 propellant at 10-in. and 12-in. diameter, to extend the SOPHY I data nearer the ideal region. Four AAB-3225 tests

each will be conducted at diameters of 6, 7, 8, 10, 12, and 24 in. The AAB-3267 material (critical diameter equals approximately 10 in.) will be tested only at 12-in. diameter and 42-in. diameter. In each series, the card-gap sensitivity will be determined out to a diameter at least four times the critical diameter.

3.2.5 Sensitivity of Unadulterated Propellant (Subtask 3.3.6)

It is the objective of this subtask to attempt to determine the minimum shock pressure required to initiate unadulterated propellant by testing subcritical samples, each containing a resistance probe along its axis. A full discussion of the method was given in Reference 2.

The constant-current power supply has been checked out. It has an excellent response to rapidly changing loads. The resistance probes have been received and inspected. Samples containing axial probes will be cast in December. The first samples will be cast with AAB-3189, since an estimate of the minimum initiating shock pressure already exists for this propellant. These tests will evaluate the hypothesis that the minimum initiating pressure can be found in subcritical testing.

4. LARGE CRITICAL-DIAMETER TESTS

4.1 GENERALIZED DETONATION MODEL

In the previously developed detonation model for RDX-adulterated propellant (Reference 4), all hot-spot initiation sites were assumed to be contributed either by RDX particles or by other inherent sites such as voids, crystal defects, or heterogeneities. For convenience, the inherent sites were considered to be of the same density and average size as the RDX particles. This assumption permitted certain simplifications in the model since the expression for the number of inherent sites could be combined with that for the number of RDX hot-spot sites into a single term.

In reality, different types of hot-spot initiating sites may vary widely with respect to average size, density, and distribution; e.g., dense RDX particles and cast-in voids. To permit consideration of such differences, the detonation model has been generalized.

The model, as reported in Reference 1, ... effective grain-burning radius R_e by

$$R_e = \frac{1}{2}\left[\frac{1}{(n_{RDX} + n_i)^{1/3}} - \bar{d}_{RDX}\right] + \frac{\bar{d}_{RDX}}{2}\left[\left(\frac{G}{\frac{f_{RDX}}{f'_{RDX}} + f'_{RDX}\frac{\rho}{\rho_{RDX}}}\right)^{1/3} - 1\right] \quad (33)$$

where

n_{RDX} = the number of RDX particles per unit mass

n_i = the number of other initiation sites per unit mass

$\bar{d}_{RDX}$ = the average diameter of the RDX particles

G = a constant

f_{RDX} = the weight fraction RDX

ρ = the density of the propellant

ρ_{RDX} = the RDX crystal density

and

f'_{RDX} = the equivalent weight fraction RDX to account for other initiation sites.

A generalized model has been developed, which in its final form states that

$$R_e = \frac{1}{2}\left[\frac{1}{\left(\sum_i^L n_j\right)^{1/3}} - \bar{d}\right] + \frac{\bar{d}}{2}\left[\left(\frac{G}{\left(\sum_i^L f_j\right)\frac{\rho}{\rho_j}\frac{\bar{d}^3}{\bar{d}_j^3}}\right)^{1/3} - 1\right] \quad (34)$$

where

L = number of different types of hot-spot initiation sites

n_j = the number of the j-th type of sites per unit mass

$\bar{d}$ = the average of the L average site diameters

f_j = the weight fraction of the j-th component

ρ_j = the density of the j-th component

and

$\overline{d^3}_j$ = the average of the cube of the L average diameters

A recent paper written by Apin and Stesik in the Russian literature (Reference 7) describes the results of their investigation of the effect that grit particles have on determining the critical diameter of an explosive. The explosive was one that reacts by a grain-burning mechanism. The results of their work are summarized by the following expression, which they derived.

$$R_e = 1/2\left[\frac{1}{(n_a + n_i)^{1/3}} - \overline{d}\right] \qquad (35)$$

where

n_a = number of added grit particles per unit mass

and

n_i = number of inherent hot-spot sites.

It can be readily seen that Equation 35 is exactly the same as the left-hand equation of Equation 34. Agreement with the Russian model lends support to the model developed on the SOPHY program. It is significant that the Russians used inert additives to increase the number of hot-spot initiation sites, since this supports the SOPHY hypothesis that included among the inherent sites are those due to heterogeneities (such as aluminum particles) in the composite propellant.

4.2 CORRECTIONS TO BLAST DATA FROM CD-96 AND CD-98

The final corrections to the blast data from the 72-in. diameter test (CD-96) and the 60-in. diameter test (CD-98) have been made. These corrections reflect the results of an intensive and thorough calibration of the pressure transducers, amplifiers, recording system, and playback system. The corrected pressures are approximately 8% lower, in the near stations, and 5% higher, in the far stations, than those reported previously as preliminary data. Table 10 shows the final blast pressure data from both tests. Figures 11 and 12 show the overpressures contributed by the propellant in Tests CD-96 and CD-98, respectively.

Table 10. Observed and Calculated Side-On Overpressure and TNT Equivalences in the 72-in. and the 60-in. Critical Diameter Tests.

Radial Distance from Charge (ft)	Radial Direction (o'clock)	Peak Side-on Overpressure * Measured (psi) 72-in. Test	Measured (psi) 60-in. Test	Calculated (psi) 72-in. Test	Calculated (psi) 60-in. Test	TNT Equivalence * From Measured Overpressure (%) 72-in. Test	From Measured Overpressure (%) 60-in. Test	From Calculated Overpressure (%) 72-in. Test	From Calculated Overpressure (%) 60-in. Test
140	2	**	127	-	-	**	203	-	-
	6	**	**	-	-	**	**	-	-
	10	**	128	-	-	**	206	-	-
250	2	50.0	30.6	-	-	195	173	-	-
	6	45.7	25.2	-	-	171	128	-	-
	10	44.5	23.8	-	-	164	116	-	-
375	2	**	**	20.2	10.7	**	**	196	128
	6	**	**	19.9	10.4	**	**	190	121
	10	**	**	19.6	10.4	**	**	186	121
500	2	9.2	6.12	-	-	140	124	-	-
	6	**	7.04	-	-	**	162	-	-
	10	**	6.90	-	-	**	156	-	-
600	2	**	**	6.86	4.11	**	**	154	103
	6	**	**	6.77	3.98	**	**	151	95
	10	**	**	6.40	4.24	**	**	135	110
700	2	5.29	3.90	-	-	159	159	-	-
	6	**	3.73	-	-	**	144	-	-
	10	5.11	3.99	-	-	148	167	-	-
1000	2	3.08	2.14	-	-	172	135	-	-
	6	3.03	2.13	-	-	165	134	-	-
	10	3.13	2.33	-	-	178	167	-	-
1500	2	1.51	**	-	-	118	**	-	-
	6	1.82	1.21	-	-	193	123	-	-
	10	1.66	**	-	-	152	**	-	-

* Measured overpressures are derived from Kistler transducer measurements. The calculated overpressures are calculated at midpoint distances between Kistler transducer stations from which time-of-arrival data are available. The calculations are performed using an equation derived from the Rankine-Hugoniot equations:

$$p = \frac{2\gamma}{\gamma + 1} P_o \left(\frac{U^2}{c_o^2} - 1 \right)$$

where p = peak overpressure on the shock front
γ = ratio of specific heats for air
P_o = test-site atmospheric pressure
U = velocity of shock front
c_o = sound velocity at test site

TNT equivalence is determined by subtracting the weight of the booster from the theoretical weight of TNT that would have given the measured (or calculated) peak side-on overpressures recorded in this table. The difference is the weight of TNT that corresponds to the propellant weight. The ratio of these two, times 100, is the TNT equivalence in percent.

* No side-on overpressure guage placed at this location.
** No data, because of gauge failure.

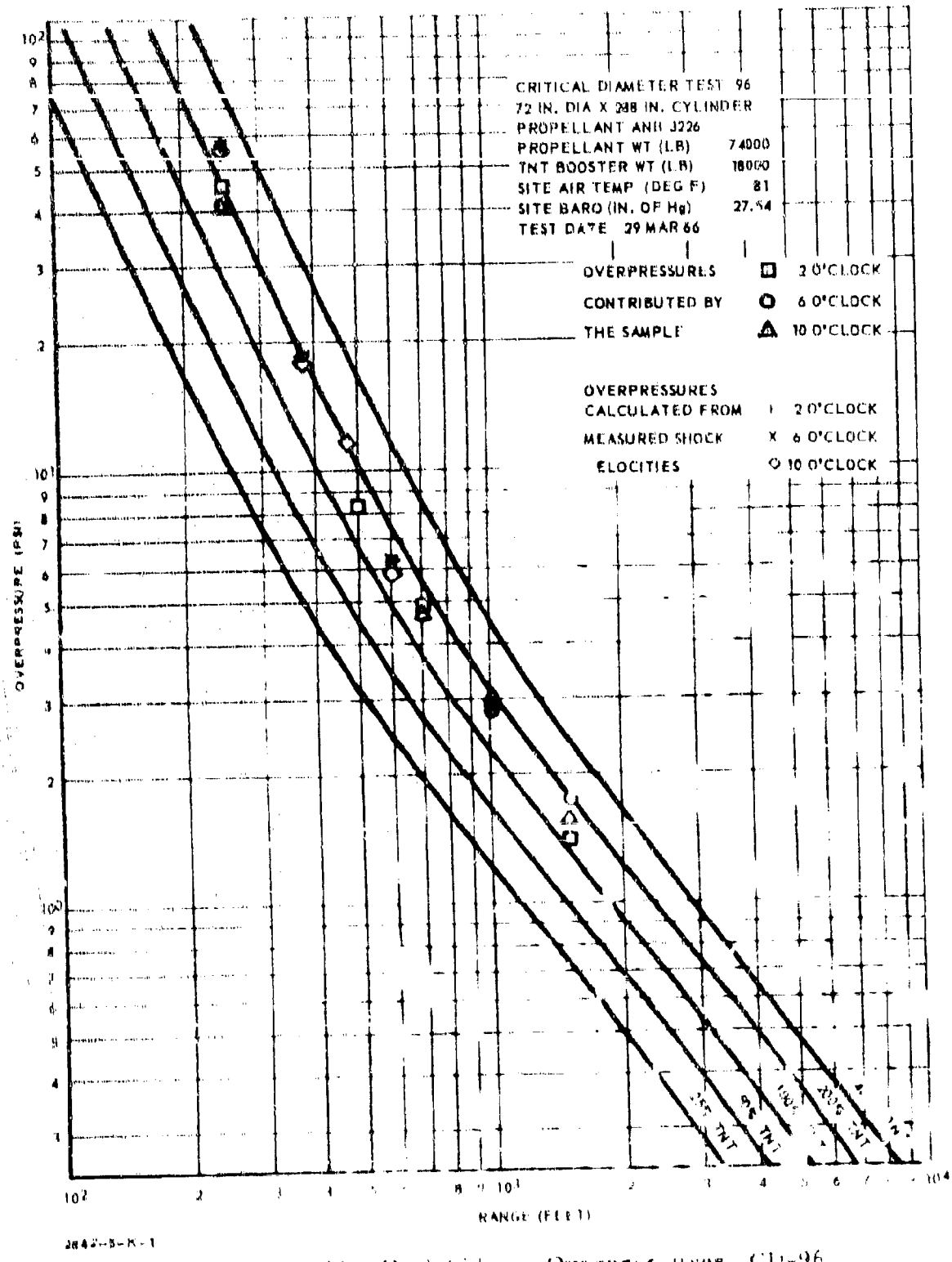

Figure 11 Peak Side-on Overpressures, CL-96.

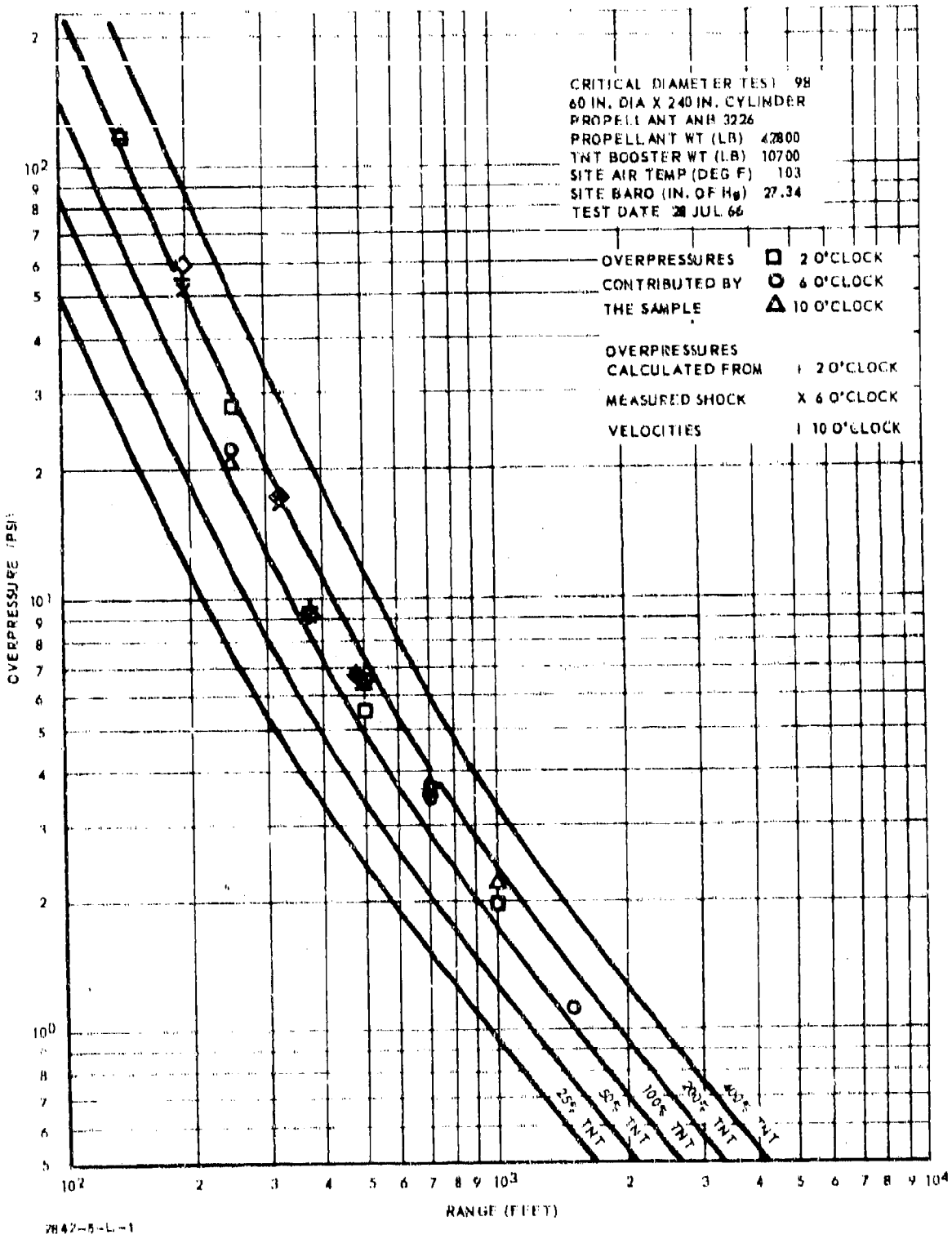

Figure 12. Peak Side-on Overpressures CD-98.

5. PROPELLANT DEFECTS STUDY

5.1 SYNTHESIS

Studies have continued to be conducted on the effects of various parameters on the quality of porous propellant. The investigations during this period have focused on (1) premix and mixing-cycle sequence, (2) Cowles Dissolver speed, (3) optimum casting vacuum, (4) introduction of blowing agents, and (5) pressure-release techniques. In addition, there has been an investigation of the relation between submix density and solid density.

5.1.1 Premix and Mixing-Cycle Sequence

The micropore content of the propellant was thought to be limited in part by those steps in the mixing cycle that require blending DER into the submix and adding aluminum to the submix to form the premix. These steps may cause breakage of the tiny bubbles that are formed during the aeration step. Four batches were prepared according to the test plan given in Table 11.

Table 11. Test Plan - Premix or Mixing Cycle Study.

Batch No.	Premix or Mixing Techniques
1-1	Cowles dissolve all ingredients except DER and oxidizer
1-2	Cowles dissolve all ingredients except oxidizer.*
1-3	Cowles dissolve all ingredients except DER and oxidizer. Aerate in the mixer with nitrogen for 30 min at 20 gas-flowmeter units.
1-4	Cowles dissolve all ingredients except oxidizer.* Aerate in the mixer with nitrogen for 30 min at 20 gas-flowmeter units.

* A cooling bath was installed for Batches 1-2 and 1-4, which permitted Cowles dissolving the catalyst into the binder with only a few degrees rise in temperature.

Following cure of these batches, samples were prepared from each batch for determination of the percent pore volume. Table 12 contains the results of these analyses. It can be seen that there was no appreciable effect on the pore volume caused by any of the variations introduced into the premix or mixing techniques. The pore content was not increased either by Cowles dissolving DER into the premix in a "complete binder" technique, or by aerating the premix in the mixer.

5.1.2 Cowles Dissolver Speed

Along with the "complete binder" technique, in which all ingredients except oxidizer are added, another study was made of the effect of Cowles Dissolver speed on the pore formation in the propellant. Three batches were cast: (1) Batch 2-1 was Cowles dissolved at 5400 rpm; (2) Batch 2-2 at 3400 rpm; and (3) Batch 2-3 at 2000 rpm. Preliminary results at the 2000-rpm level show incomplete dispersion of ingredients. Therefore, future work will be done at higher speeds to assure complete mixing under all conditions. Table 13 shows the results of this investigation. The percent pores were found to increase with increases in the Cowles dissolver speed.

5.1.3 Casting-Vacuum Study

Casting of large samples cannot be made free of large casting pores when vibration alone is used. Therefore it is desirable to determine the highest possible casting vacuum that will not destroy the micropores created in the propellant but will prevent formation of casting pores (herein referred to as macropores). The results shown in Tables 12 and 13 indicate that a casting vacuum of 25-in. Hg does destroy a large percentage of these micropores.

A subsequent casting of a batch prepared by aerating with nitrogen through a sintered-glass funnel for 12 hr at ambient temperature, was carried out at 20-in. Hg. The percent pore volume was significantly improved over that obtained at 25-in. Hg vacuum, but the vacuum is still too high. Cured at 20-in. Hg, the propellant had a 2.8% pore volume (at temperatures of 110°F and 135°F) and a 1.8% pore volume (at cure temperature of 150°F), compared to a 6.0% pore volume when cured at 110°F under no vacuum.

Table 12. Effect of Premix or Mixing Cycle Changes on Propellant Pore Volume.

Batch No.	Casting Vacuum (in. Hg)	Cure Temp (°F)	Propellant Density (gm/ml)	Pore Volume (%)
1-1	No vacuum	110	1.6382	5.4
	25	110	1.6754	3.3
	25	135	1.6852	2.7
	25	150	1.6928	2.2
1-2	No vacuum	110	1.6478	4.9
	25	110	1.6823	2.0
	25	135	1.7190	0.8
	25	150	1.7185	0.9
1-3	No vacuum	110	1.6477	4.9
	25	110	1.7215	0.7
	25	135	1.7187	0.8
	25	150	1.7199	0.7
1-4	No vacuum	110	1.6396	5.3
	25	110	1.7188	0.8
	25	135	1.7213	0.6
	25	150	1.7249	0.4

Table 13. Effect of Cowles Dissolver Speed on Percentage of Pore Content

("Complete Binder" Method)

Cowles Dissolver Speed (rpm)	Casting Vacuum (in. Hg)	Cure Temp (°F)	Propellant Density (gm/ml)	Pore Volume (%)
5400	No vacuum	110	1.6357	5.6
	25	110	1.7129	1.1
	25	135	1.7178	0.9
	25	150	1.7304	0.1
3400	No vacuum	110	1.6362	5.5
	25	110	1.7263	0.4
	25	135	1.7213	0.6
	25	150	1.7239	0.5
2000	No vacuum	110	1.6413	5.1
	25	110	1.7185	0.8
	25	135	1.7238	0.5
	25	150	1.7223	0.6

More batches were cast of ANB-3226 propellant, under casting-vacuum conditions that varied from 10- to 29-in. Hg. The cured samples were analysed for percent pore volume, and the percent of total potential pore content was calculated using that achieved at the ambient-pressure casting as the reference. Figure 13 shows the results of this analysis. The data indicate that a vacuum of less than 10-in. Hg will not affect the micropore content appreciably. However, it was also noted at this low vacuum level that the macropores are not removed. It is possible that vibration during casting would improve this condition.

5.1.4 Blowing Agents

Several blowing agents were used to produce gas in the propellant, for the purpose of increasing the pore formation. These agents were of two types: those that vaporize easily (chloroform, methylchloroform, and Freon-TF) and those that either react or decompose to form a gas (toluene diisocyanate/water and hydroxylamine acid sulfate). The first type of blowing agent is more feasible since the blowing effect can be controlled more readily by the vacuum and temperature of the mixing, casting, and curing operations.

Chloroform was incorporated at 2 and 4% by weight of binder, and the effects on the pore content were determined from samples cast and cured under various conditions of temperature and pressure. The results are given in Table 14. A slight improvement over the control (14.9% vs 13.4% pore content) was observed when propellant containing 4% weight chloroform was cured at 110°F under atmospheric pressure. Curing at 150°F did not increase the pore content. Under vacuum, the porosity increased.

The ANB-3226 propellants containing Freon-TF and methylchloroform (at 4% weight of binder) were mixed in a similar fashion. The results are shown in Table 15. Where indicated, the propellants were cured at 110°F for 24 hr and 48 hr under atmospheric pressure prior to vacuum cure, to prevent surface bubbling. Neither of these two agents were as effective as chloroform in causing pore formation.

Neither toluene diisocyanate (TDI)/water nor hydroxylamine acid sulfate were effective at the levels used: 0.05 and 0.1% weight of propellant for TDI/water; 0.05, 0.1, and 0.2 meq hydroxylamine acid sulfate per gram of Paracril in the binder. The TDI/water combination forms carbon dioxide gas, and the hdyroxylamine acid sulfate reacts with Paracril to generate nitrogen decomposition products. At the 0.2 meq/g level, the hydroxylamine acid sulfate shortened the propellant pot life to the extent that the batch was uncastable.

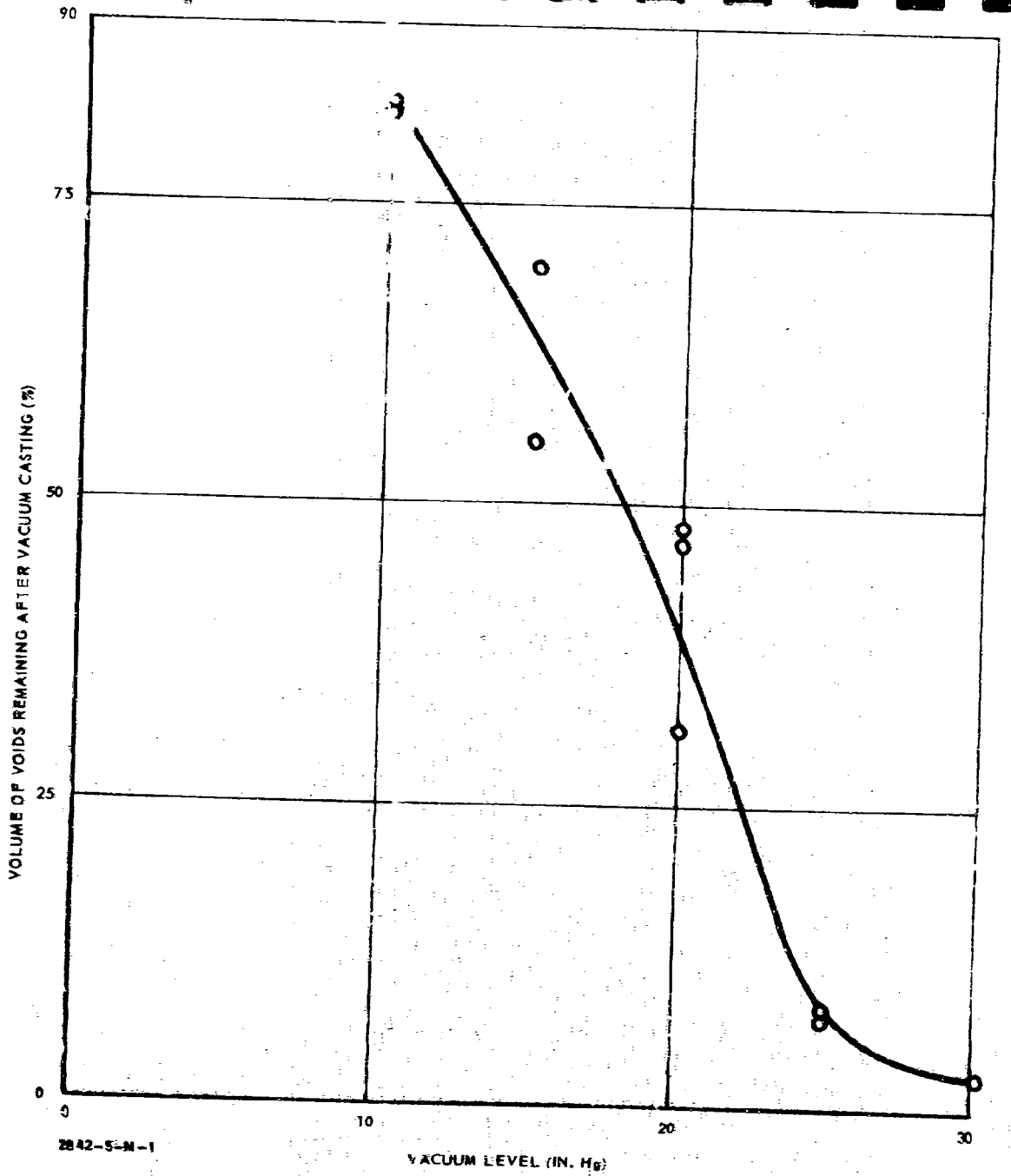

Figure 13. Effect of Vacuum Level During Casting on Pore Foundation.

Table 14. Effect of Chloroform on Pore Content.

Chloroform % by Wt of Binder	Cure Temp (°F)	Casting Vacuum (in. Hg)	Cure Vacuum (in. Hg)	Pore Volume (%)
0 (control)	110	None	None	13.4
2	110	None	None	14.1
	110	15	None	9.7
	150	None	None	13.0
	150	15	None	5.9
4	110	None	None	14.9
	110	15	15*	11.1
	150	None	None	14.1
	150	15	15*	11.8

*During the vacuum cure, the propellant surface rose and bubbled over.

Table 15. Effect of Freon-TF and Methylchloroform on Pore Content.*

Ingredient	Cure Temp (°F)	Casting Vacuum (in. Hg)	Cure Vacuum (in. Hg)	Pore Volume (%)
(Control)	110	None	None	13.4
Freon-TF	110	None	None	13.0
	110	None	5	10.1
	110	None	5**	10.5
	110	None	10	10.0
Methylchloroform	110	None	None	12.4
	110	10	10**	11.6
	110	10	10***	10.6
	150	10	5	9.0

* 4% by weight of binder
** After 24 hr at atmospheric pressure
*** After 48 hr at atmospheric pressure

5.1.5 Gas-Pressure Technique

ANB-3226 binder was subjected to 3000 psig of nitrogen for periods of 3 to 24 hr prior to propellant mixing, to dissolve nitrogen in the binder. The results of this effort, (Table 16), show that a pore content of 15.3% was obtained under these conditions; i.e., 24 hr of binder exposure to 3000 psig nitrogen, 15-in. Hg vacuum during both cast and cure, and a cure temperature of 150°F. Propellant was also mixed in the normal manner, then it was subjected to 3000 psig nitrogen for 16 hr prior to cure. The effect of this treatment was to increase the pore content of the cured propellant to 11.7- 13.6 compared with the 7.0-9.3% found in the control.

5.1.6 Comparison of Submix Density to Solid Density

If the measurement of the submix density before mixing could be correlated with the subsequent propellant solid densities, a qualification criterion could be established prior to mixing. Submix densities were determined on five batches prior to mixing. Subsequent measurement of the solid densities of the propellants did not correlate with the submix densities found prior to mixing. These data are shown in Table 17. This table also indicates that no significant increase in percent pore volume is achieved by the elimination of the aluminum addition step.

5.2 ANALYSIS

Various techniques to provide an accurate estimate of the total surface area of cracked propellant are being evaluated, as the initial effort toward developing methods for total characterization of such samples. A method has been perfected for microscopically determining the percent pore volume and pore-diameter distribution in porous propellant. Data for this new analytical method will be reported in the subsequent reports. Progress in the surface-area studies is discussed in the following subparagraphs.

5.2.1 Moisture-Adsorption Technique

Measurements were made of the water vapor equilibrium curves of propellant samples prepared with different total surface areas. Three samples were prepared from cubes of propellant. Sample A was composed of cubes 2.24 mm/side, having a specific area of $16.7 \times 10^{-4} m^2/g$.

Table 16. Effect of Dissolved Nitrogen on Pore Content.

Exposure Time at 3000 psig Nitrogen (hr)	Cure Temp (°F)	Casting Vacuum (in. Hg)	Cure Vacuum (in. Hg)	Pore Volume (%)
0 (control)	110	None	None	13.4
3	110	None	None	13.3
	110	10	10	11.4
	150	None	None	13.1
	150	10	10	8.2
12	110	None	None	14.0
	110	10	10	8.8
	150	None	None	13.0
	150	10	10	7.7
15	110	None	None	12.5
	110	15	15	7.0
	150	None	None	12.7
	150	15	15	15.3
24	110	None	None	12.1
	110	15	15	9.5
	150	None	None	11.5
	150	15	15	15.1

Table 17. Effect of Submix and Mixing Conditions on Pore Volume.

Batch No.	Submix Density (gm/ml)	Cure Temp (°F)	Propellant Density (gm/ml)	Pore Content (%)	Remarks
3-1	0.8515	110	1.6539	4.5	Low-density submix
	0.8515	135	1.6648	3.8	
	0.8515	150	1.6715	3.4	
3-2	0.9260	110	1.6488	4.8	High-density submix
	0.9260	135	1.6628	3.7	
	0.9260	150	1.6621	4.0	
3-3	0.8475	110	1.6340	5.7	Control for new submix
	0.8475	135	1.6483	4.8	
	0.8475	150	1.6523	4.6	
3-4	0.9145	110	1.6441	5.1	Same as 3-3 except Al is added with DER
	0.9145	135	1.6512	4.6	
	0.9145	150	1.6530	4.5	
3-5	0.8406	110	1.6309	5.8	Same as 3-4 except new submix and new day of mixing is involved (control).
	0.8406	135	1.6411	5.2	
	0.8406	150	1.6581	3.0	

Sample B, 4.25 mm/side, had a specific area of 8.1×10^{-4} m^2/g. Sample C, was composed of cubes 7.63 mm/side and had a specific area of 6.5×10^{-4} m^2/g.

The samples were weighed in covered weighing bottles, using an analytical balance. Weight-vs time curves were obtained by exposing the samples in the weighing bottles to controlled atmospheres of 60% relative humidity and 0% relative humidity. The moisture adsorption was both rapid and reversible. The moisture-time curves are shown in Figure 14. The three samples can be readily distinguished by the initial rate of change or by the rate of approach to equilibrium.

5.2.2 Gas Chromatography

An attempt has been made to use propellant samples as a chromatographic column. The cut samples are packed in glass tubes 3-in. long x 1/2-in. OD and placed in a dry air stream. Controlled amounts of water vapor are injected upstream of the propellant. A moisture detector, placed at the exit end of the sample tube, supplies an electrical output related to the water-vapor content of the air stream. Lack of reproducibility was experienced, and the problem has been traced to small leaks in the system where Tygon tubing and rubber stoppers were employed. A more permanent apparatus is now under construction.

5.2.3 Gas Adsorption

The surface-area measurements of propellant by gas adsorption requires an apparatus that consists of a gas burette, sample container, liquid container for vapor delivery, and a manifold with vacuum stopcocks to isolate the components of the system. Gases are discharged by displacement from the gas burette, using a mercury column connected by rubber tubing to a mercury reservoir. The sample is exposed to gas at pressure P, which is maintained by delivering gas from the burette as adsorption occurs in the test cell. The amount of gas adsorbed at the sample surface is determined by the total delivered volume of gas minus that quantity that is adsorbed on the walls of the cell and that which occupies the free space within the cell. The correction factors are determined independently by making blank runs, using nitrogen with and without the sample, and using water without the sample.

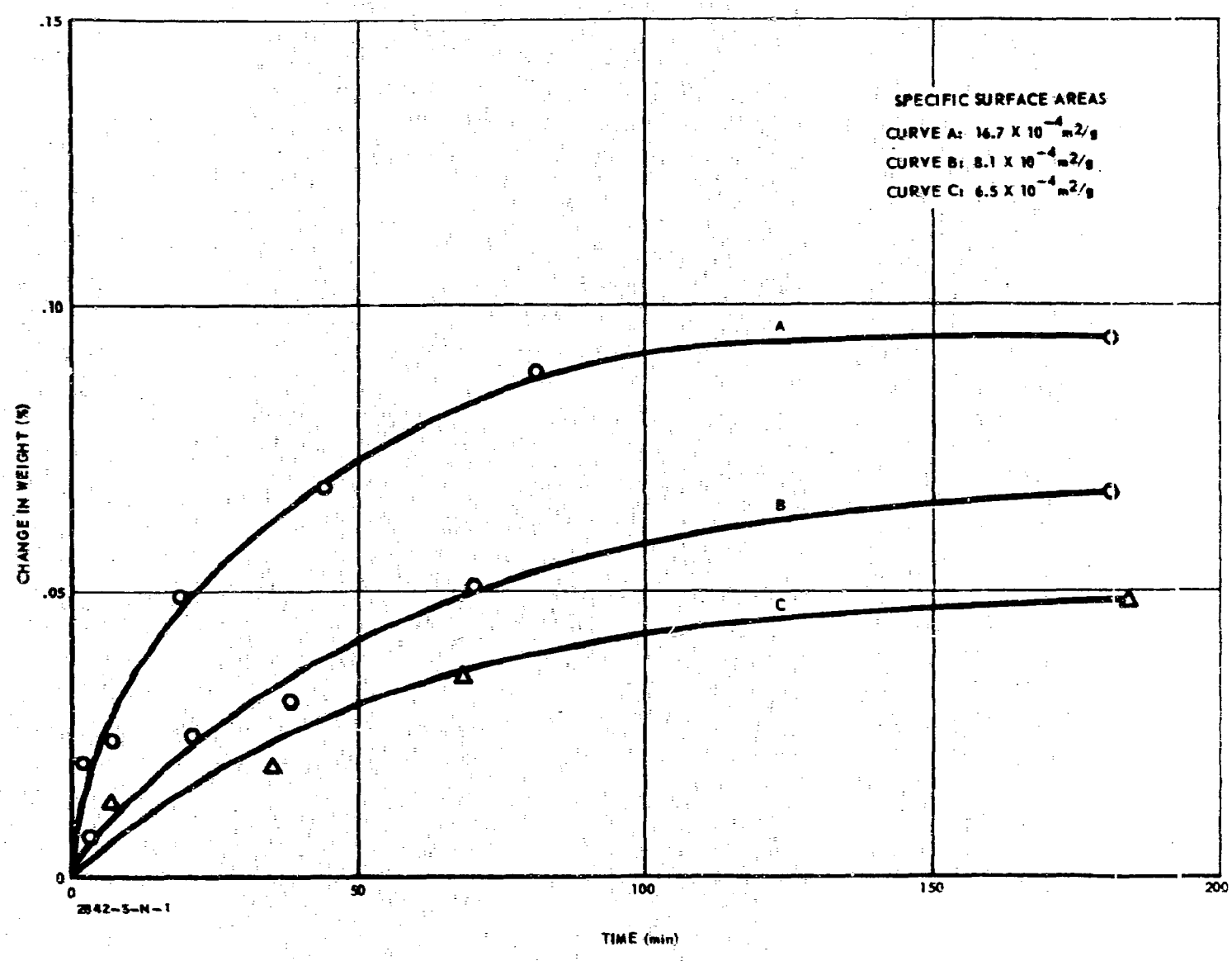

Figure 14. Effect of Surface Area in Water Vapor Equilibrium Curves.

The results from the first two samples that have been tested are shown in Figure 15. The data scatter is mainly due to inability to make the low-pressure measurements to the required degree of precision. It appears that this method can detect differences in surface area. Difficulties with diffusion into the propellant, which had been expected, have not materialized at the low relative humidities involved.

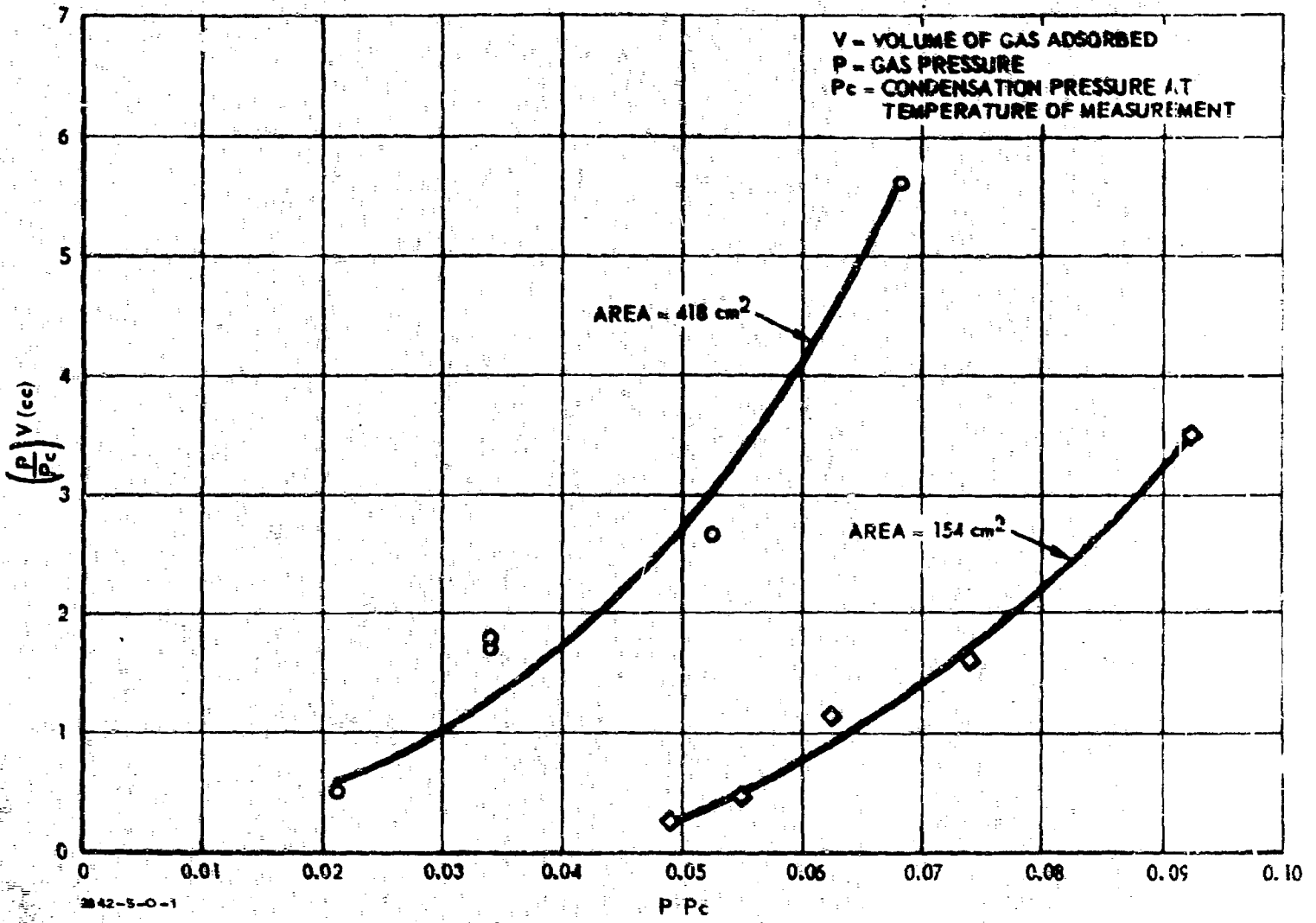

Figure 15. Water Vapor Adsorption By Cut Propellant Surfaces.

REFERENCES

1. Program Plan - Project SOPHY - Solid Propellant Hazards Program, Aerojet-General Report 0977-01(01)ER, 14 December 1965.

2. [illegible] SOPHY - Solid Propellant Hazards Program, Technical Documentary Report AFRPL-TR-66-26, Aerojet General Report 0977-01(04)QP, 29 September 1966.

3. Jones, H., "A Theory of the Dependence of the Rate of Detonation of Solid Explosives on the Diameter of the Charge," Proc Roy Soc (London), Vol. 189A, pp415-426, 1947.

4. Large Solid-Propellant Boosters Explosive Hazards Study Program (Project SOPHY), Technical Documentary Report AFRPL-TR-65-211, Aerojet-General Report 0866-01(01)FP, 24 November 1965.

5. Irwin, O. R., P. K. Salzman, and W. H. Andersen, "Deflagration Characteristics of Ammonium Perchlorate at High Pressures," Ninth Symposium (International) on Combustion, Academic Press, New York. pp 358-365. 1963.

6. Analysis of Shock Attenuation of 0.5- and 2.0-in. Diameter Card-Gap Sensitivity Tests, Aerojet-General Report SRP 289 (Special), January 1962.

7. Apin, A. Ya., and L. N. Stesik, "Mechanism of the Chemical Reaction in the Detonation of Solid Explosives," Z. prik. mekh. tekh. fiz., No. 2, pp 146-149. 1965.

BLANK PAGE

UNCLASSIFIED

DOCUMENT CONTROL DATA - R&D

(Security classification of title, body of abstract and indexing annotation must be entered when the overall report is classified)

1 ORIGINATING ACTIVITY (Corporate author) Aerojet-General Corporation Downey, California 90241	2a REPORT SECURITY CLASSIFICATION Unclassified 2b GROUP N/A

3 REPORT TITLE

Project SOPHY - Solid Propellant Hazards Program

4 DESCRIPTIVE NOTES (Type of report and inclusive dates)

Progress Report 1 September - 30 November 1966

5 AUTHOR(S) (Last name, first name, initial)

Elwell, R. B.
Salzman, P. K.
Vail, R. W., Jr.

6 REPORT DATE	7a TOTAL NO OF PAGES	7b NO OF REFS
December 1966	80	

8a CONTRACT OR GRANT NO.	9a ORIGINATOR'S REPORT NUMBER(S)
AF04(611)10919 b PROJECT NO 63A00201 c d	0977-01(05)QP 9b OTHER REPORT NO(S) (Any other numbers that may be assigned this report) AFRPL-TR-66-276

10 AVAILABILITY/LIMITATION NOTICES

Qualified requestors may obtain copies of this report from DDC.

11 SUPPLEMENTARY NOTES	12 SPONSORING MILITARY ACTIVITY
	AFRPL, Hazards Analysis Branch, AF Systems Command, Edwards, AFB, Edwards, California 93523

13 ABSTRACT

A correlation is reported that evaluates the use by the Aerojet detonation model of the modified Jones model, to describe nonideal detonation characteristics of solid-composite propellant.

An analysis of the perturbation of the detonation process in hollow cylindrical charges is presented. The critical geometries of triangular and rectangular columns have been found to be 95 and 94% of the critical diameter, respectively. The pseudocritical geometries (defined in this report) for circular-core and cross-core hollow cylinders both are 88% of the critical diameter. The Hugoniot of AAB-3225 propellant (adulterated propellant containing 7.1% RDX) is reported. A generalized expression for the effective grain radius has been developed. Corrected values of the peak overpressure data from the two large critical-diameter tests of unadulterated propellant (72-in. diameter and 60-in. diameter) are reported. Progress has been made in determining the effect of several processing parameters on the quality of cast porous propellant. Techniques to measure the surface area of cracked propellant samples are being evaluated.

DD FORM 1 JAN 64 1473

UNCLASSIFIED

14 KEY WORDS	LINK A		LINK B		LINK C	
	ROLE	WT	ROLE	WT	ROLE	WT
Propellant Hazards **Critical Geometry** **Jetting Phenomena** **Critical Diameter** **Sensitivity** **SOPHY**						

INSTRUCTIONS

1. **ORIGINATING ACTIVITY:** Enter the name and address of the contractor, subcontractor, grantee, Department of Defense activity or other organization *(corporate author)* issuing the report.

2a. **REPORT SECURITY CLASSIFICATION:** Enter the overall security classification of the report. Indicate whether "Restricted Data" is included. Marking is to be in accordance with appropriate security regulations.

2b. **GROUP:** Automatic downgrading is specified in DoD Directive 5200.10 and Armed Forces Industrial Manual. Enter the group number. Also, when applicable, show that optional markings have been used for Group 3 and Group 4 as authorized.

3. **REPORT TITLE:** Enter the complete report title in all capital letters. Titles in all cases should be unclassified. If a meaningful title cannot be selected without classification, show title classification in all capitals in parenthesis immediately following the title.

4. **DESCRIPTIVE NOTES:** If appropriate, enter the type of report, e.g., interim, progress, summary, annual, or final. Give the inclusive dates when a specific reporting period is covered.

5. **AUTHOR(S):** Enter the name(s) of author(s) as shown on or in the report. Enter last name, first name, middle initial. If military, show rank and branch of service. The name of the principal author is an absolute minimum requirement.

6. **REPORT DATE:** Enter the date of the report as day, month, year, or month, year. If more than one date appears on the report, use date of publication.

7a. **TOTAL NUMBER OF PAGES:** The total page count should follow normal pagination procedures, i.e., enter the number of pages containing information.

7b. **NUMBER OF REFERENCES:** Enter the total number of references cited in the report.

8a. **CONTRACT OR GRANT NUMBER:** If appropriate, enter the applicable number of the contract or grant under which the report was written.

8b, 8c, & 8d. **PROJECT NUMBER:** Enter the appropriate military department identification, such as project number, subproject number, system numbers, task number, etc.

9a. **ORIGINATOR'S REPORT NUMBER(S):** Enter the official report number by which the document will be identified and controlled by the originating activity. This number must be unique to this report.

9b. **OTHER REPORT NUMBER(S):** If the report has been assigned any other report numbers *(either by the originator or by the sponsor)*, also enter this number(s).

10. **AVAILABILITY/LIMITATION NOTICES:** Enter any limitations on further dissemination of the report, other than those imposed by security classification, using standard statements such as:

(1) "Qualified requesters may obtain copies of this report from DDC."

(2) "Foreign announcement and dissemination of this report by DDC is not authorized."

(3) "U. S. Government agencies may obtain copies of this report directly from DDC. Other qualified DDC users shall request through _____."

(4) "U. S. military agencies may obtain copies of this report directly from DDC. Other qualified users shall request through _____."

(5) "All distribution of this report is controlled. Qualified DDC users shall request through _____."

If the report has been furnished to the Office of Technical Services, Department of Commerce, for sale to the public, indicate this fact and enter the price, if known.

11. **SUPPLEMENTARY NOTES:** Use for additional explanatory notes.

12. **SPONSORING MILITARY ACTIVITY:** Enter the name of the departmental project office or laboratory sponsoring *(paying for)* the research and development. Include address.

13. **ABSTRACT:** Enter an abstract giving a brief and factual summary of the document indicative of the report, even though it may also appear elsewhere in the body of the technical report. If additional space is required, a continuation sheet shall be attached.

It is highly desirable that the abstract of classified reports be unclassified. Each paragraph of the abstract shall end with an indication of the military security classification of the information in the paragraph, represented as *(TS)*, *(S)*, *(C)*, or *(U)*.

There is no limitation on the length of the abstract. However, the suggested length is from 150 to 225 words.

14. **KEY WORDS:** Key words are technically meaningful terms or short phrases that characterize a report and may be used as index entries for cataloging the report. Key words must be selected so that no security classification is required. Identifiers, such as equipment model designation, trade name, military project code name, geographic location, may be used as key words but will be followed by an indication of technical context. The assignment of links, rules, and weights is optional.